

Fast and Scalable Spike and Slab Variable Selection in High-Dimensional Gaussian Processes

Hugh Dance

University College London

Brooks Paige

University College London

Abstract

Variable selection in Gaussian processes (GPs) is typically undertaken by thresholding the inverse lengthscales of ‘automatic relevance determination’ kernels, but in high-dimensional datasets this approach can be unreliable. A more probabilistically principled alternative is to use spike and slab priors and infer a posterior probability of variable inclusion. However, existing implementations in GPs are extremely costly to run in both high-dimensional and large- n datasets, or are intractable for most kernels. As such, we develop a fast and scalable variational inference algorithm for the spike and slab GP that is tractable with arbitrary differentiable kernels. We improve our algorithm’s ability to adapt to the sparsity of relevant variables by Bayesian model averaging over hyperparameters, and achieve substantial speed ups using zero temperature posterior restrictions, dropout pruning and nearest neighbour mini-batching. In experiments our method consistently outperforms vanilla and sparse variational GPs whilst retaining similar runtimes (even when $n = 10^6$) and performs competitively with a spike and slab GP using MCMC but runs up to 1000 times faster.

riodicity) through flexible choice of covariance function $k(x, x')$ (Rasmussen and Williams, 2006), without parametrically restricting the function class.

To infer variable relevance in GPs ‘automatic relevance determination’ (ARD) kernels are often implemented, which use per-dimension inverse lengthscale parameters $\{\theta_j\}_{j=1}^d$ as a relevance measure. Learning $\{\theta_j\}_{j=1}^d$ by maximum marginal likelihood (ML-II) often sees $\theta_j \rightarrow 0$ for irrelevant dimensions due to the marginal likelihood’s intrinsic complexity penalty. This makes it trivial to select relevant variables by thresholding $\{\theta_j\}_{j=1}^d$ (Rasmussen and Williams, 2006). However, we find this shrinkage does not hold sufficiently in high-dimensional input designs to enable reliable threshold placement. This agrees with recent evidence (Ober et al., 2021; Mohammed and Cawley, 2017) that demonstrates the marginal likelihood can overfit in heavily parameterised regimes.

An alternative approach is to place spike and slab priors on the inverse lengthscales and infer a per-variable posterior inclusion probability (PIP). Existing implementations in GPs perform excellently but either use Markov Chain Monte Carlo (MCMC) schemes which are very costly to run in high-dimensional or large- n datasets (Savitsky et al., 2011), or are only tractable for specific kernels (Dai et al., 2015).

Our contribution: We develop a fast and scalable variational inference algorithm for GPs with spike and slab variable selection priors, which we call the spike and slab variational Gaussian process (SSVGP). By using a continuous approximation to a Dirac spike and a specific factored variational approximation, we are able to derive an otherwise intractable approximate co-ordinate ascent variational inference (CAVI) (Blei et al., 2017) algorithm with similar complexity to ML-II training, that can be used with arbitrary differentiable kernels. We subsequently improve our algorithm’s ability to adapt to the sparsity in the data by Bayesian model averaging over spike and slab hyperparameter values, and use a combination of zero temperature posterior restrictions, dropout pruning,

1 Introduction

Gaussian processes (GPs) are a powerful Bayesian nonparametric approach to regression used widely in machine learning and statistics. GPs enable the user to encode prior information about a function $f(\cdot)$ they aim to approximate (eg. stationarity, smoothness, pe-

and nearest neighbour minibatching to achieve substantial speed ups and $\mathcal{O}(nf(n)d)$ scalability, where $f(n) \in [\log(n), n]$. Our method can be used to enhance predictive accuracy of GP regression in high-dimensional scenarios, or enable probabilistically principled variable selection through inference on the PIPs - without the usual implementation costs of spike and slab priors in non-conjugate models.

We find across a range of experiments that our SSVGP consistently outperforms standard GP regression and sparse variational GP regression (Titsias, 2009; Hensman et al., 2013) in terms of predictive accuracy whilst keeping similar runtimes, outperforms benchmark variable selection algorithms, and can match the performance of a spike and slab GP with MCMC (Savitsky et al., 2011) but can run up to 1000 times faster.

2 Background and related work

In this section we review GP regression, spike and slab priors and related work.

2.1 Gaussian process regression

A Gaussian process is a random function $f \sim \mathcal{GP}(m(\mathbf{x}), k_{\alpha}(\mathbf{x}, \mathbf{x}'))$ with mean function $m(\cdot) : \mathcal{X} \rightarrow \mathbb{R}$ and positive semi-definite covariance function (‘kernel’) $k(\cdot, \cdot) : \mathcal{X} \times \mathcal{X} \rightarrow \mathbb{R}$, with the property that any finite subset of points are multivariate Gaussian: $\mathbf{f} = [f(\mathbf{x}_1), \dots, f(\mathbf{x}_n)] \sim \mathcal{N}(\mathbf{m}, K_{XX})$, where $[\mathbf{m}]_i = m(\mathbf{x}_i)$ and $[K_{XX}]_{ij} = k_{\alpha}(\mathbf{x}_i, \mathbf{x}_j)$. Here α parameterises the kernel.

Given a dataset $\mathcal{D} = (\mathbf{y}, X) \in \mathbb{R}^n \times \mathbb{R}^{n \times d}$, we define a Gaussian process model as follows:

$$\begin{aligned} \mathbf{y} | \mathbf{f} &\sim p(\mathbf{y} | \mathbf{f}) \\ f(\cdot) | \alpha &\sim \mathcal{GP}(m(\mathbf{x}), k_{\alpha}(\mathbf{x}, \mathbf{x}')) \end{aligned}$$

In standard GP regression (GPR), the observation model is a Gaussian centred at \mathbf{f} : $p(\mathbf{y} | \mathbf{f}) = \prod_{i=1}^n \mathcal{N}(y_i | f_i, \sigma^2)$. In this case the marginal likelihood $p(\mathbf{y} | \alpha)$ has closed form and can be maximised to learn kernel parameters α and noise variance σ^2 (aka ML-II optimisation). Predictive moments at unknown locations $\mathbf{x}_* \in \mathbb{R}^d$ can also be derived in closed form (Rasmussen and Williams, 2006).

To do variable selection in GPR, automatic relevance determination (ARD) kernels (MacKay et al., 1998) are often used which contain per-dimension inverse lengthscales $\{\theta_j\}_{j=1}^d$, to be used as a measure of variable relevance (assuming inputs are scaled to have unit variance). Most popular ARD kernels (e.g. squared exponential (SE), Matérn, Cauchy) fall into a subclass of

anisotropic stationary kernels of the form:

$$k_{\tau, \theta}(\mathbf{x}, \mathbf{x}') = \tau h(\|\theta \odot (\mathbf{x} - \mathbf{x}')\|_2) \quad (1)$$

Here $\tau > 0$ is the scale parameter of the kernel and $h(\cdot)$ is a continuous (often monotonic) function. ML-II optimisation often sees $\{\theta_j\} \rightarrow 0$ for irrelevant dimensions due to the intrinsic complexity penalty in the marginal likelihood (Rasmussen and Williams, 2006), and so variable selection can be undertaken by hard-thresholding $\{\theta_j\}_{j=1}^d$. However, we demonstrate that ML-II optimisation can insufficiently shrink inverse lengthscales in high-dimensional designs making it challenging to infer an appropriate threshold.

We note better measures of variable relevance have been developed (Paananen et al., 2019), however these approaches are not ideal for high-dimensional variable selection as there is no obvious way to convert the relevance scores into binary selection decisions.

2.2 Spike and slab priors

Spike and slab priors are considered a gold standard for high-dimensional variable selection problems due to their excellent properties (Narisetty and He, 2014), empirical performance and interpretability. Given a model $p(\mathbf{y} | \theta)$ with per-dimension ‘relevance’ parameters $\theta \in \Theta \subset \mathbb{R}^d$, a spike and slab prior augments the model with binary inclusion variables $\gamma \in \{0, 1\}^d$:

$$p(\theta, \gamma) = \prod_{j=1}^d [\mathcal{P}_{slab}(\theta_j) \pi]^{\gamma_j} [\mathcal{P}_{spike}(\theta_j) (1 - \pi)]^{1 - \gamma_j}$$

Here $\mathcal{P}_{slab}(\cdot)$ is the slab distribution (usually set to be approximately uniform), and $\mathcal{P}_{spike}(\theta_j)$ is the spike distribution (usually set to be a point mass at zero (Mitchell and Beauchamp, 1988) or a continuous approximation to a point mass (George and McCulloch, 1997)), and π is the prior probability of inclusion. Since $\gamma_j = 0$ implies $\theta_j \approx 0$, variable relevance can be inferred through the posterior inclusion probability (PIP) $p(\gamma_j = 1 | \mathbf{y})$ for input dimension j :

$$p(\gamma_j = 1 | \mathbf{y}) = \frac{\sum_{\gamma_{-j}} \int_{\theta} p(\mathbf{y} | \theta) p(\theta, \gamma)}{\sum_{\gamma} \int_{\theta} p(\mathbf{y} | \theta) p(\theta, \gamma)}$$

This quantity is often intractable but can be approximated using MCMC (Ishwaran and Rao, 2005) or variational inference (Carbonetto and Stephens, 2012).

2.3 Related work on spike and slab GPs

Several MCMC schemes have been developed for spike and slab priors in GPs (Linkletter et al., 2006; Savitsky et al., 2011; Qamar and Tokdar, 2014). Whilst performance is typically excellent, these algorithms are

costly to run both in large- d datasets as they stochastically search over a 2^d model space, and in large- n datasets as they use many model evaluations with $\mathcal{O}(n^3)$ cost. For example, [Savitsky et al. \(2011\)](#) report runtimes of nearly 3 hours when $(n = 100, d = 1000)$.

[Dai et al. \(2015\)](#) instead use variational inference with spike and slab priors for latent dimensionality selection in the GP latent variable model (GP-LVM). They use a paired mean field (PMF) variational approximation $q(\theta_j|\gamma_j)q(\gamma_j) = \mathcal{N}(\theta_j|\mu_j, \sigma_j^2)^{\gamma_j} \delta_0(\theta_j)^{1-\gamma_j}$ and sparse variational GP approximation [Titsias \(2009\)](#) to reduce complexity to $\mathcal{O}(nm^2)$ for m inducing points. Whilst their approach could in principle be modified for supervised GPR, the bound they optimise is only tractable for a few specific kernels, of which the most popular (the SE kernel) requires $m = \mathcal{O}(\log^d(n))$ inducing points for a high quality posterior approximation ([Burt et al., 2019](#)) - which is exponential in d .

By contrast to previous work, our method is generally faster than stochastic variational GPR ([Hensman et al., 2013](#)) on datasets up to $n = 10^6$, has $\leq \mathcal{O}(n^2d)$ complexity and works with any differentiable kernel.

3 The spike and slab variational Gaussian process

In this section we derive our baseline algorithm and approach to scaling to large- n datasets. We then derive a Bayesian Model averaging (BMA) procedure to improve our algorithm’s adaptability to the degree of sparsity in relevant inputs, and speed up our algorithm in substantially using several modifications. We demonstrate performance throughout using a toy example. For key equation derivations see the appendix.

3.1 Model and inference algorithm

Unlike previous spike and slab GP implementations, we place a spike and slab prior on the inverse lengthscales where both the spike and slab are Gaussian as in [George and McCulloch \(1997\)](#). This enables a fast and otherwise intractable approximate co-ordinate ascent variational inference (CAVI) ([Blei et al., 2017](#)) algorithm to be used for fast posterior inference. We also place a Beta prior over the prior inclusion probability. This induces the following generative model:

$$\begin{aligned} p_\phi(\mathbf{y}|\boldsymbol{\theta}) &= \mathcal{N}(\mathbf{y}|\boldsymbol{\theta}, \tilde{K}_{XX}) \\ p(\theta_j, \gamma_j|\pi) &= \left[\mathcal{N}\left(\theta_j|0, \frac{1}{cv}\right) \pi \right]^{\gamma_j} \left[\mathcal{N}\left(\theta_j|0, \frac{1}{v}\right) (1-\pi) \right]^{1-\gamma_j} \\ p(\pi) &= \text{Beta}(\pi|a, b) \end{aligned}$$

Here $\boldsymbol{\theta} \in \mathbb{R}^d$ are the inverse lengthscales, $\phi = \{\tau, \sigma^2\} \in \mathbb{R}_{>0}^2$ are the scale and noise parameters, $\gamma \in$

$\{0, 1\}^d$ are the binary inclusion indicators, $[\tilde{K}_{XX}]_{ij} = k_{\tau, \boldsymbol{\theta}}(\mathbf{x}_i, \mathbf{x}_j) + \delta_1(i=j)\sigma^2$, $v \gg 1$ is the precision of the spike distribution, and $cv \ll 1$ is the precision of the slab distribution.

We use variational inference to approximate the posterior using factored variational approximation: $p_\phi(\boldsymbol{\theta}, \gamma, \pi|\mathbf{y}) \approx q(\boldsymbol{\theta})q(\gamma)q(\pi)$ and thus minimise the Kullback Liebler divergence $KL[q(\boldsymbol{\theta})q(\gamma)q(\pi)||p(\boldsymbol{\theta}, \gamma, \pi|\mathbf{y})]$. This is equivalent to maximising the following lower bound on the log evidence $\log p(\mathbf{y})$ ([Blei et al., 2017](#)):

$$\mathcal{F} = \langle \log p(\mathbf{y}|\boldsymbol{\theta}) \rangle_{q(\boldsymbol{\theta})} - KL[q(\boldsymbol{\theta})q(\gamma)q(\pi)||p(\boldsymbol{\theta}, \gamma, \pi)] \quad (2)$$

Importantly, by using this factorisation and the continuous spike, exact co-ordinate ascent (CAVI) updates for $q(\gamma)$, $q(\pi)$ are available (we parameterise $q(\boldsymbol{\theta})$ such that $\langle \theta_j^2 \rangle_{q(\boldsymbol{\theta})}$ has closed form):

$$\begin{aligned} q^*(\gamma_j) &= \text{Bern}(\gamma_j|\lambda_j) \\ \lambda_j &= \left(1 + c^{-\frac{1}{2}} e^{-\frac{1}{2} \langle \theta_j^2 \rangle_{q(\boldsymbol{\theta})} + \langle \log(\frac{1-\pi}{\pi}) \rangle_{q(\pi)}} \right)^{-1} \quad (3) \end{aligned}$$

$$\begin{aligned} q^*(\pi) &= \text{Beta}(\pi|\xi_a, \xi_b) \\ (\xi_a, \xi_b) &= (a + \sum_{j=1}^d \lambda_j, b + d - \sum_{j=1}^d \lambda_j) \quad (4) \end{aligned}$$

Note $\lambda_j = q(\gamma_j = 1)$ is the PIP for dimension j . Whilst the same does not hold for $q(\boldsymbol{\theta})$ due to the non-conjugacy of the model, for a suitable parametric restriction $q_\psi(\boldsymbol{\theta})$ we can approximate its co-ordinate update using stochastic gradient optimisation of \mathcal{F} with the reparameterisation trick ([Kingma and Welling, 2013](#)). Whilst the gradient of the KL term has closed form, the gradient of the expected likelihood term $\nabla_\psi \langle \log p(\mathbf{y}|\boldsymbol{\theta}) \rangle_{q_\psi(\boldsymbol{\theta})}$ needs approximating. The reparameterisation trick enables us to do this unbiasedly by parameterising $q_\psi(\cdot)$ such that $\boldsymbol{\theta} = \mathcal{T}_\psi(\epsilon)$, where $\mathcal{T}_\psi(\cdot)$ is differentiable, $\epsilon \sim q(\epsilon)$ and $q(\epsilon)$ does not depend on ψ . In this case, given S samples $\epsilon^{(1:S)} \sim q(\epsilon)$, $\nabla_\psi \mathcal{F}$ can be unbiasedly approximated as:

$$\begin{aligned} \hat{\nabla}_\psi \mathcal{F} &= \frac{1}{S} \sum_{s=1}^S (\nabla_\theta \log p_\phi(\mathbf{y}|\boldsymbol{\theta}^{(s)}) \nabla_\psi \mathcal{T}_\psi(\epsilon^{(s)}) \\ &\quad - \nabla_\psi KL[q(\boldsymbol{\theta})q(\gamma)||p(\boldsymbol{\theta}|\gamma)]) \quad (5) \end{aligned}$$

Scale and noise parameters ϕ can be optimised jointly using a similar unbiased approximation:

$$\hat{\nabla}_\phi \mathcal{F} = \frac{1}{S} \sum_{s=1}^S \nabla_\phi \log p_\phi(\mathbf{y}|\boldsymbol{\theta}^{(s)}) \quad (6)$$

Thus, our approximate CAVI algorithm (a-CAVI) iterates between (1) *exactly* maximising \mathcal{F} with respect to $\{q(\gamma), q(\pi)\}$ using eq. 3 and 4, and (2) *approximately* maximising \mathcal{F} with respect to $\{q_\psi(\boldsymbol{\theta}), \phi\}$ using gradient based optimisation with eq. 5, 6: and 7:

$$(\psi, \phi) \leftarrow (\psi, \phi) + \boldsymbol{\eta} \odot (\hat{\nabla}_\psi \mathcal{F}, \hat{\nabla}_\phi \mathcal{F}) \quad (7)$$

Algorithm 1 summarises the steps. In practice we set learning rates η using ADAM (Kingma and Ba, 2014) and set $q(\theta)$ as a Mean Field Gaussian (MFG), so $q(\epsilon) = \mathcal{N}(\mathbf{0}, I)$ and $\mathcal{T}_\psi(\epsilon) = \sigma \odot \epsilon + \mu$. Fortunately reparameterisation gradient variance is sufficiently low such that setting $S = 1$ enables efficient learning.

Algorithm 1: a-CAVI for SSVGP training

Input : Data: (\mathbf{y}, X) , initialisation:
 $(\psi^{(0)}, \lambda^{(0)}, \xi^{(0)}, \phi^{(0)})$, learning rates: η ,
hyperparameters: (v, c, a, b) , # a-CAVI
iters: K , # gradient iters: T , # MC
samples: S

```

1 for  $K$  iterations do
2   for  $T$  steps do
3     sample  $\epsilon^{(1:S)} \sim \mathcal{N}(\mathbf{0}, I)$ .
4     get  $\hat{\nabla}_\psi \mathcal{F}, \hat{\nabla}_\phi \mathcal{F}$  using eq. 5 and 6.
5     update  $(\psi, \phi)$  using equation 7.
6   end
7   update  $\lambda$  using equation 3.
8   update  $\xi$  using equation 4.
9 end
Output:  $\psi, \lambda, \xi, \phi$ 

```

Complexity analysis: When $q(\theta)$ is MFG and $S = 1$, gradients 5 and 6 cost $\mathcal{O}(n^3)$ for inverting K_{XX} and $\mathcal{O}((n^2 + 1)d)$ for matrix-vector products, which is similar complexity to ML-II gradients. The remaining CAVI updates for $q(\gamma)$, $q(\pi)$ are $\mathcal{O}(d)$ and generally extremely cheap to perform. If we had instead used a Dirac spike and/or PMF approximation as in Dai et al. (2015), then no exact CAVI updates would be tractable and only score gradients (i.e. BBVI (Ranganath et al., 2014)) would be available to optimise $q(\gamma)$, which typically require $S \gg 1$ samples per iteration for efficient learning (Mohamed et al., 2020). Table 1 demonstrates our method significantly outperforms a Dirac spike with PMF+BBVI on a toy example whilst retaining much faster runtimes.

Predictions: At test time, given S_* samples $\theta^{(1:S_*)} \sim q_\psi(\theta)$ and learned ϕ , the predictive distribution can be approximated by a discrete mixture of standard GPR posterior predictives $\{p_\phi(y_* | \mathcal{D}, \mathbf{x}_*, \theta^{(s)})\}_{s'=1}^{S_*}$, which has closed form moments (see the appendix):

$$p(y_* | \mathcal{D}, \mathbf{x}_*) \approx \sum_{s'=1}^{S_*} p_\phi(y_* | \mathcal{D}, \mathbf{x}_*, \theta^{(s')}) \quad (8)$$

Interpreting the factorisation: Our factorisation over inverse lengthscales θ and inclusion variables γ mean that $q(\gamma)$ is not used at test time. Whilst this may seem counterintuitive, note that $q(\theta)$ automatically embeds in information from $q(\gamma)$ during a-CAVI iterations in ‘message passing’ fashion. In the

MFG case, the KL term acts as an L2-regulariser on $\psi = \{\mu, \sigma\}$, where the penalty scale varies with λ :

$$\nabla_\mu KL[q(\cdot) || p(\cdot)] = -v\mu \odot (c\lambda + \mathbf{1} - \lambda) \quad (9)$$

$$\nabla_\sigma KL[q(\cdot) || p(\cdot)] = -v\sigma \odot (c\lambda + \mathbf{1} - \lambda) + \sigma^{-1} \quad (10)$$

As a result, when $\lambda_j \approx 0$, we often have $\mu, \sigma \rightarrow 0$ for large enough spike precision v . Thus, our algorithm can be interpreted as adaptively regularising the posterior over inverse lengthscales based on learned PIPs.

3.2 Scaling to large-n datasets

Since our algorithm suffers $\mathcal{O}(n^3)$ complexity, in large- n datasets we use the approach taken by Chen et al. (2020) of approximating $\nabla \log p_\phi(\mathbf{y} | \theta)$ at each iteration using a rescaled m -sized minibatch comprised of a uniformly sampled point and its $m - 1$ nearest neighbours: $\frac{n}{m} \nabla \log p_\phi(\mathbf{y}_{nn} | \theta)$. This reduces the inversion complexity bottleneck to $\mathcal{O}(m^3)$ at the expense of an $\mathcal{O}(nd)$ nearest neighbour search. Although minibatch gradients are biased due to the non-decomposable likelihood, Chen et al. (2020) were able to outperform a range of state-of-the-art scalable GP approximations on various datasets, and their approach is easily integrated into our base algorithm. When the kernel is monotonically decreasing in a distance metric, we use this metric to find the neighbours with the posterior means $\langle \theta \rangle_{q(\theta)} = \mu$ in place of inverse lengthscales θ . For example using kernels of the form given in eq. 1 we use distance metric $d(\mathbf{x}, \mathbf{x}') = \|\mu \odot (\mathbf{x} - \mathbf{x}')\|_2$.

Since making predictions also suffers an $\mathcal{O}(n^3)$ inversion cost, in $n \gg 10^4$ datasets we follow Jankowiak and Pleiss (2021) and truncate our approximate predictive distribution in eq. 8 using m_* nearest neighbours of \mathbf{x}_* . We again use the distance metric in the kernel when available but replace μ with $\theta^{(s)}$ in each mixture component. This reduces inversion complexity to $\mathcal{O}(S_* m_*^3)$ per test point, again at the expense of an $\mathcal{O}(S_* nd)$ nearest neighbour search.

3.3 Toy example demonstration

We now demonstrate our SSVGP on a toy example where we draw $n = 300$ samples of 100-dimensional input $\mathbf{x} \sim \mathcal{N}(\mathbf{0}, I)$ and set response using 5/100 inputs as $y = \sum_{j=1}^5 \sin(a_j x_j) + \epsilon$, where $\{a_j\}$ are grid spaced over $[0.4, 1]$, and the noise to signal ratio is set to 0.05. We set spike precision to $v = 10^4$ and slab precision to $cv = 10^{-4}$, and set Beta prior hyperparameters uninformatively to $a = b = 10^{-3}$. For comparison we implement an ML-II GP using GPytorch (Gardner et al., 2018) and a spike and slab GP using the Dirac spike and PMF variational factorisation trained using BBVI. See the appendix for implementation and experiment details. In all cases the SE kernel is used.

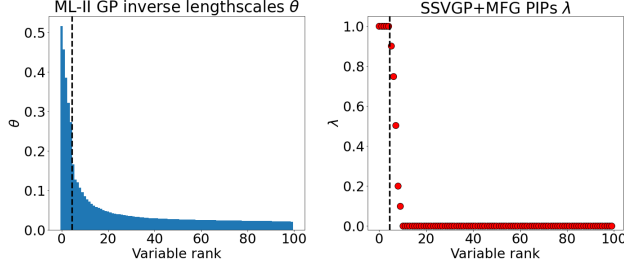


Figure 1: Toy example size ordered profile for ML-II GP inverse lengthscales (LHS) and SSVGP+MFG PIPs (RHS). First 5 variables (LHS of black dashed line) are constrained to be the 5 relevant variables. Profiles averaged over 10 trials. Whilst the ML-II GP profile fails to shrink many irrelevant inverse lengthscales, the SSVGP learns to exclude nearly all irrelevant variables with high probability and includes all relevant variables with near certainty.

Table 1 displays (normalised) mean squared error (MSE) and runtime (mean \pm sd) obtained on 10 trials using $n_* = 100$ test points. Our SSVGP outperforms both ML-II and PMF-BBVI on average, and is much closer in runtime to the ML-II GP. In Fig. 1 we also highlight how our SSVGP enables much more reliable variable selection than the ML-II GP by better distinguishing between irrelevant and relevant variables.

4 Bayesian model averaging for adaptive sparsity

One issue is that the learned model sparsity (via PIPs) is heavily dependent on spike and slab parameter v . This can be seen by analysing the ‘posterior point of intersection’ (PPI), which is the value of transformed expected sufficient statistic $\hat{\theta} := \sqrt{\langle \theta^2 \rangle_{q(\theta)}}$ that induces an even chance of inclusion $\lambda = \frac{1}{2}$ in the a-CAVI update for $q(\gamma)$ (derived in the appendix):

$$\hat{\theta} = \sqrt{\frac{\log\left(\frac{1}{c}\right) + 2\left(\log\frac{1-\pi}{\pi}\right)_{q(\pi)}}{v(1-c)}} \quad (11)$$

The PPI only adapts with $q(\pi)$ during training and the degree of adaptability is relatively limited (see the appendix). As a result, since the PPI is $\mathcal{O}(v^{-\frac{1}{2}})$, v can entirely determine the sparsity of the PIPs. This is demonstrated in Table 2, which shows that when we run our SSVGP on the same 10 trials increasing v from 10^2 to 10^6 , the average recovered PIP increases from 0 to 1. We therefore need a reliable way of adapting v to the input sparsity in the data for our method to be useful in practice.

We found directly maximising \mathcal{F} with respect to v (or variational posterior $q(v)$) lead to highly initialisation

Method	MSE	Runtime (s)
ML-II GP	0.096 ± 0.014	5.0 ± 0.7
PMF+BBVI(10)	0.088 ± 0.019	71.6 ± 1.6
PMF+BBVI(100)	0.077 ± 0.013	595.3 ± 4.9
SSVGP+MFG	0.068 ± 0.011	27.8 ± 0.5

Table 1: Toy example mean \pm sd results (10 trials) for ML-II GP, Dirac spike and slab GP with PMF+BBVI using 10 and 100 score-grad samples respectively, and SSVGP with Mean Field Gaussian $q(\theta)$.

v	10^2	10^3	10^4	10^5	10^6
average PIP	0	0.05	0.07	0.34	1

Table 2: Toy example average PIP recovered for SSVGP with varying spike and slab parameter v .

dependent results, and so did not address the problem. Our solution is to instead train a set of models $\{\mathcal{M}_k\}_{k=1}^K$ with different scale parameters $v_k \in \mathcal{V}$, and Bayesian model average over the learned posteriors $\{q_k(\theta)\}_{k=1}^K, \{q_k(\gamma)\}_{k=1}^K$ using approximate posterior model probabilities $w_k \approx p(\mathcal{M}_k|\mathbf{y})$. Marginal PIPs $\{\bar{\lambda}_j\}_{j=1}^d = \{\sum_{k=1}^K \lambda^{(k)} w_k\}_{j=1}^d$ can then be used to infer variable relevance and do variable selection.

However, for this procedure to work we need (1) a fast enough algorithm to enable multiple (> 10) trials without compromising speed and scalability, and (2) a good approximation to the posterior model probability $p(\mathcal{M}_k|\mathbf{y})$. We address each of these aspects below.

4.1 Speeding up the a-CAVI algorithm

We first modify our a-CAVI algorithm to enable order of magnitude speed-ups, whilst only negligibly impacting performance when v is appropriately set.

Zero-temperature restrictions: We zero-temperature restrict the inverse lengthscale posterior: $q(\theta) = \delta_{\mu}(\theta)$. This eliminates the need for Monte-Carlo sampling at training and test time as both the expected likelihood term $\langle p_{\phi}(\mathbf{y}|\theta) \rangle_{q(\theta)}$ and predictive distribution are now tractable (see the appendix).

Dropout pruning: We use a form of dropout pruning on variables with small PIPs during training iterations. This type of procedure has been used to great effect in sparsifying neural networks whilst only negligibly impacting performance (Louizos et al., 2017). Specifically after every a-CAVI iteration, we permanently enforce $\langle \theta_j \rangle = \mu_j = 0$ if $\lambda_j \leq \epsilon$ for some chosen $\epsilon \in (0, 1)$. This reduces training complexity with respect to input dimensionality from $\mathcal{O}(d)$ to $\mathcal{O}(p_t)$, where $p_t = \{\#\lambda_j^{(t)} \geq \epsilon\}$, leading to dramatic speed ups when few inputs are relevant. Moreover, we prove in

	MF	ZT	ZT+drop	ZT+drop(m=n/4)
MSE	0.068	0.068	0.064	0.065
avg PIP	0.07	0.05	0.06	0.05
Runtime(s)	27.8	24.1	10.5	1.3

Table 3: Toy example average results for SSVGP implementing a-CAVI modifications sequentially (left to right). Using all modifications speeds up runtime by $\sim 20\times$, whilst performance remains similar.

the appendix that under certain conditions if $v(1 - \epsilon)$ is large enough, pruning will only negligibly affect converged solutions of a-CAVI.

We also use $m < n$ nearest neighbour minibatching to improve runtime even when $n < 10^3$ as we find for large enough m (e.g. $m \geq \frac{n}{4}$) this can improve performance. We argue this is because in this scenario the gradient bias remains low and so the intrinsic regularisation benefits of SGD (Smith et al., 2021) can be leveraged with minimal cost. Table 3 demonstrates the obtainable speed ups using these modifications on the toy example, with pruning threshold $\epsilon = 0.5$ and $m = \frac{n}{4}$ minibatching. Whilst average performance remains similar, average runtime drops to 1.3s.

4.2 Approximating posterior model weights with leave-one-out log predictive density

Rather than use the evidence lower bound \mathcal{F} to approximate the log posterior model probability (under a uniform prior over models $F_k \leq \log p(\mathcal{M}_k|\mathbf{y})$) we follow Yao et al. (2018) and use the leave-one-out log predictive density (LOO-LPD): $\sum_{i=1}^n \log p(y_i|\mathcal{D}_{-i}, \mathcal{M}_k)$. This is because \mathcal{F} 's preference for sparsity is heavily influenced by hyperparameter c , as there is a fixed variable inclusion cost of $\log(\frac{1}{c})$ (see the appendix), making model weights overly dependent on c . Moreover, the LOO-LPD is more robust against overfitting and model mis-specification than the log evidence (Jankowiak and Pleiss, 2021; Gelman et al., 2014).

In our case under the ZT posterior, inverse lengthscales $\boldsymbol{\theta}$ can be treated as parameters fixed at $\boldsymbol{\mu}_k$ for model \mathcal{M}_k . In this case the LOO-LPD for \mathcal{M}_k is that of a standard GP evaluated at $(\boldsymbol{\theta} = \boldsymbol{\mu}_k, \phi = \phi_k)$ (derived in the appendix). To compute the LOO-LPD in efficient $\mathcal{O}(n^3)$ time in small datasets we use the Bürkner et al. (2021) algorithm, which uses rank 1 updates to K_{XX} . In large datasets we nearest-neighbour truncate the LOO-LPD following the success of this approach in Jankowiak and Pleiss (2021). That is, for each (y_i, \mathbf{x}_i) , we condition on \tilde{m} nearest neighbours of \mathbf{x}_i found using the distance metric in the kernel. This reduces complexity to $\mathcal{O}(m^3n)$ but introduces an $\mathcal{O}(nf(n)p_k)$ query cost, where p_k is the count of non-pruned variables in model \mathcal{M}_k and $f(n) \in [\log(n), n]$ is the query

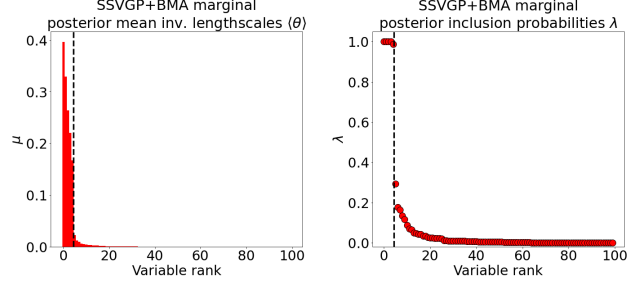


Figure 2: Toy example average size ordered profiles for (LHS) SSVGP+BMA posterior mean inverse lengthscales and (RHS) SSVGP+BMA PIPs. The PIP profile is better than the SSVGP+MFG (Fig. 1) and the posterior mean inverse lengthscales are shrunk to near-zero for all irrelevant dimensions due to the regularisation from $\{q_k(\gamma)\}_{k=1}^K$ and learned model weighting.

Method	MSE	MCC	Runtime (s)
ML-II GP	0.096 \pm 0.014	-	5.0 \pm 0.7
PMF+BBVI(100)	0.077 \pm 0.013	0.62 \pm 0.06	595.3 \pm 4.9
SSVGP+MFG	0.068 \pm 0.011	0.82 \pm 0.09	27.8 \pm 0.5
SSVGP+BMA	0.064 \pm 0.01	0.98 \pm 0.04	14.6 \pm 0.4

Table 4: Toy example mean \pm sd results. SSVGP+BMA outperforms all other methods in predictive accuracy (MSE) and variable selection accuracy (MCC), and runs in similar time to ML-II GP.

cost using Ball-trees (Omohundro, 1989) or KD-trees (Bentley, 1975) (our preferred algorithms).

Given the recovered posteriors and model weights, the predictive distribution is a discrete mixture of standard GP predictive posteriors evaluated at $\{\boldsymbol{\mu}_k, \phi_k\}$:

$$p(\mathbf{y}_*|X_*, \mathcal{D}) \approx \sum_{k=1}^K \int p_{\phi_k}(\mathbf{y}_*|X_*, \boldsymbol{\theta}, \mathcal{D}) q_k(\boldsymbol{\theta}) d\boldsymbol{\theta} w_k \\ = \sum_{k=1}^K p_{\phi_k}(\mathbf{y}_*|X_*, \boldsymbol{\theta} = \boldsymbol{\mu}_k, \mathcal{D}) w_k \quad (12)$$

To speed up prediction time we stochastically threshold weights by drawing $\mathbf{z} \sim \text{Multi}(\mathbf{w}, S)$ and setting $\mathbf{w} \propto \mathbf{z}$, for $S \geq 100$, and when predictive accuracy is the core focus we simply select the best model. We again use nearest-neighbour truncation when $n > 10^4$.

4.3 Demonstrating BMA on the toy example

We demonstrate our SSVGP with BMA on the same 10 trials of the toy example using 11 values of v grid spaced over $10^4 \times 2^{\{-\log_2(1000), \log_2(1000)\}}$ such that $10^1 \leq v \leq 10^7$, and use the ZT posterior with $m = \frac{n}{4}$ minibatching and pruning threshold $\epsilon = 0.5$.

We display in Table 4 performance results against previous models and in Fig. 2 the average profile of PIPs

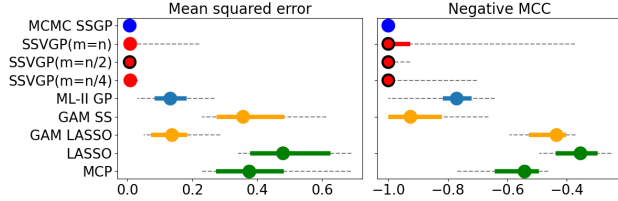


Figure 3: Experiment 1 median (circle), 25-75 percentiles (line), and 10-90 percentiles (dashed line) results. Black border denotes best median performance. Left is better. SSVGPs outperform all implemented comparators and can match single trial of Savitsky et al. (2011) MCMC spike and slab GP.

MCMC	SSVGP(n)	SSVGP(n/2)	SSVGP(n/4)	ML-II
10224s	20.3s	11.0s	8.4s	3.9s

Table 5: Experiment 1 average runtimes for different methods and single trial time of Savitsky et al. (2011) spike and slab GP when running 5×10^5 MCMC iters.

and posterior mean inverse lengthscales. Note we also report the Matthews Correlation Coefficient (MCC $\in [-1, 1]$) (Matthews, 1975) to measure variable selection accuracy when using $\bar{\lambda} = 0.5$ as an inclusion threshold. Our SSVGP with BMA outperformed all other methods in terms of predictive and variable selection accuracy, learned a better quality PIP profile than the original SSVGP+MFG without BMA and also ran faster on average ($\sim 15s$). Thus, our BMA procedure and a-CAVI modifications induced better and faster performance than using our original algorithm with a well calibrated choice of v .

5 Experiments

We now test our SSVGP in several experiments (we use BMA with ZT and dropout by default from now on). We consider a synthetic small- n experiment, a synthetic large- n experiment and benchmark real datasets. See the appendix for experiment and implementation details. The SE kernel is used throughout, but our method works with any differentiable kernel.

5.1 Experiment 1: a small-scale, high dimensional variable selection problem

We first test our SSVGP on 50 replications of Savitsky et al. (2011) main experiment to assess whether our algorithm can compete with their spike and slab GP using a Dirac spike and MCMC. The experiment draws $n = 100$ training and $n_* = 20$ test samples of $d = 1000$ dimensional inputs $\mathbf{x} \sim \text{Unif}[0, 1]^d$ and sets the response as an additive function of 6/1000 inputs:

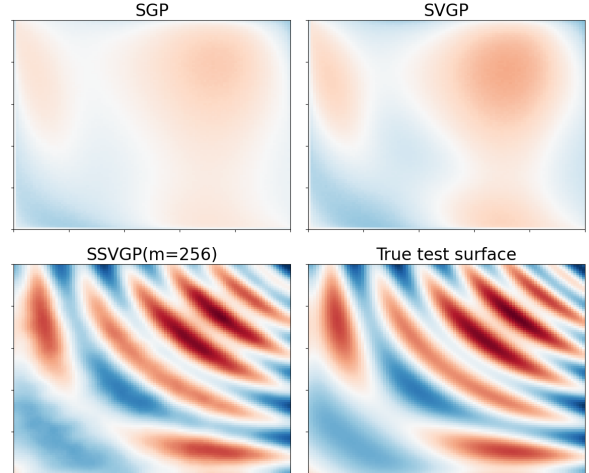


Figure 4: Experiment 2 average prediction surfaces as a function of the two relevant inputs when $n = d = 10^4$, and true test surface for latent (noiseless) \mathbf{f}_* . The SGP and SVGP cannot accurately recover the surface due to the number of noise dimensions, whilst our SSVGP recovers a near perfect surface.

$y = x_1 + x_2 + x_3 + x_4 + \sin(3x_5) + \sin(5x_6) + \epsilon$ for $\epsilon \sim \mathcal{N}(0, 0.05)$. We also implement the ML-II GP and several benchmark variable selection algorithms: LASSO (Tibshirani, 1996), MCP (Zhang, 2010), GAM with group LASSO penalty (Huang et al., 2009) and GAM with group spike and slab LASSO penalty (Bai et al., 2020). We implement our SSVGP with mini-batch sizes $m \in \{\frac{n}{4}, \frac{n}{2}, n\}$ and the same settings as previously. For the ML-II GP we report MCC using the best performing threshold from $0.1^{0,0.5,1,1.5,2}$ as indicative 'best-case' performance with thresholding.

In Fig. 3 and Table 5 we present MSE, negative MCC and runtime percentiles for all models against Savitsky et al. (2011) single completed trial. All SSVGPs outperformed the implemented comparators, and the median trial performance is near identical to the single trial of Savitsky et al's MCMC spike and slab GP but with average runtimes of $< 20s$ rather than $> 10000s$. When $m = \frac{n}{2}$ performance is best but $m = \frac{n}{4}$ outperformed $m = n$ on average (see appendix for details).

5.2 Experiment 2: A large-scale sparse prediction challenge

We next test the scalability and predictive performance of our method in a large-scale synthetic experiment against the Sparse GP (SGP) of Titsias (2009) and the Stochastic Variational GP (SVGP) of Hensman et al. (2013), as two popular best-practice benchmarks in the scalable GP literature. We generate synthetic data from a 2d input interactive function

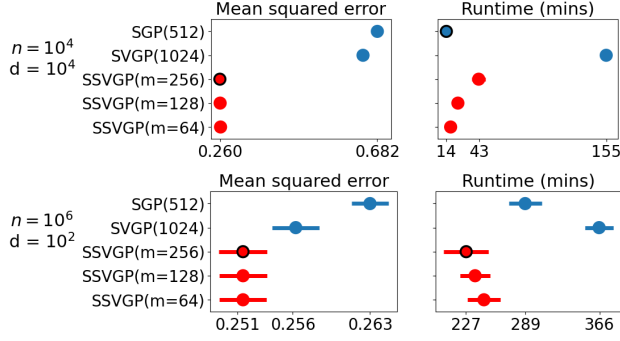


Figure 5: Experiment 2 mean (circle) \pm standard deviation (line) results. Black border denotes best on average. Our SSVGPs perform better on average and produce competitive runtimes. Note $m = 256$ is fastest when $n = 10^6$ as runtime is dominated by LOO-LPD computation, and since $m = 256$ selected fewer variables per model in BMA this reduced compute time.

$y(\mathbf{x}) = \tan(x_1) + \tan(x_2) + \sin(2\pi x_1) + \sin(2\pi x_2) + \cos(4\pi^2 x_1 x_2) + \tan(x_1 x_2) + \epsilon$ where the noise to signal ratio is set to $\frac{1}{3}$ and $x_1, x_2 \sim \mathcal{U}[0, 1]$. We then augment with $d - 2$ noise dimensions correlated 0.5 with x_1, x_2 . We fix $nd = 10^8$ and run 3 trials of (i) An ultra-high dimensional design ($n = 10^4, d = 10^4$), and (ii) a one million training point design ($n = 10^6, d = 10^2$). We test on $n_* = 10^4$ datapoints but with x_1, x_2 grid spaced on $[0, 1]$. We implement the SGP and SVGP using GPyTorch (Gardner et al., 2018) with 512 and 1024 inducing points respectively consistent with standard practice (Chen et al., 2020; Wang et al., 2019; Jankowiak and Pleiss, 2021). We implement the SSVGP with $m = \{64, 128, 256\}$ minibatch sizes, and use 64 and 256 neighbours in LOO-LPD and predictive distribution truncation respectively. In Figure 4 we present average prediction surfaces as a function of the two relevant inputs, against the latent test function f_* . Figure 5 displays MSE and runtime results.

Our SSVGPs outperformed the SGP and SVGP on average in both designs and consistently ran faster than the SVGP. Whilst the MSE improvement is minimal in the ($n = 10^6, d = 10^2$) case, when $n = d = 10^4$ the SGP and SVGP fail to achieve competitive performance. This demonstrates the gains to using our method as input dimensionality and sparsity grows. SSVGP performance is similar across minibatch sizes, but $m = 256$ is best as expected.

Computational cost: As n grows, SSVGP runtime is dominated by LOO-LPD computation due to the $\mathcal{O}(nf(n)p_k)$ nearest neighbour search cost where $f(n) \in [\log(n), n]$ depending on p_k ($\#$ non-pruned variables in model k). As p_k grows, complexity converges to $\mathcal{O}(n^2 p_k)$ and so in large- p_k scenarios our

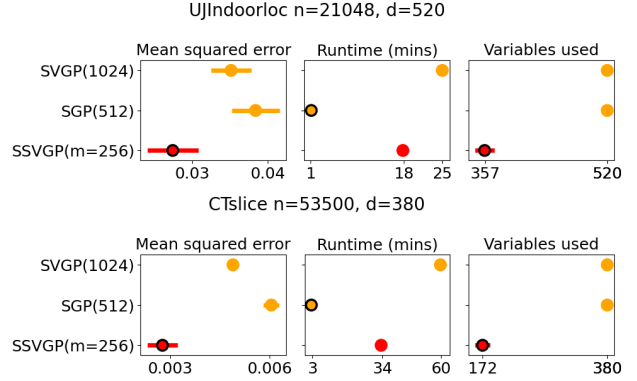


Figure 6: Real dataset mean (circle) \pm standard deviation (line) results on CTslice and UJindoorloc. Black border denotes best average performance. The SSVGP outperformed both the SGP and SVGP whilst predicting with a sparse subset of identified relevant variables.

method may be slower than the SVGP when $n \gg 10^6$. However in scenarios where $p_k \ll 100$ for most of the K models in BMA we expect our method to remain faster than SVGP even when $n \gg 10^6$.

5.3 UCI repository datasets

We test our method on two high-dimensional datasets from the UCI repository (UJINDOORLOC (n, d) = (21048, 583) and CTSLICE (n, d) = (53500, 380)). We implement the SSVGP with $m = 256$ minibatching, and again use 64 and 256 nearest neighbours respectively in LOO-LPD and predictive distribution truncation. In Figure 6 we produce MSE and runtime results from 10 trials of random 4:1 training/test splits, and compare against the the SGP(512) and SVGP(1024). Our SSVGP performed best on average in both datasets and again ran faster than the SVGP.

6 Conclusion

We introduced the spike and slab variational Gaussian process (SSVGP): a fast and scalable training and inference method for Gaussian processes with spike and slab variable selection priors. Unlike previous spike and slab GP implementations, our method runs in similar time to sparse variational GPs even on $n = 10^6$ sized datasets, and works with any differentiable kernel. Thus, our SSVGP captures the variable selection and predictive accuracy benefits of spike and slab priors over ARD in high-dimensional designs, without the typical inference cost in GPs. Future research could explore Bayesian optimisation (Shahriari et al., 2015) for efficient model search, or extensions to classification and deep kernel learning (Wilson et al., 2016).

References

- Bai, R. (2021). Spike-and-slab group lasso for consistent estimation and variable selection in non-gaussian generalized additive models.
- Bai, R., Moran, G. E., Antonelli, J. L., Chen, Y., and Boland, M. R. (2020). Spike-and-slab group lassos for grouped regression and sparse generalized additive models. *Journal of the American Statistical Association*, pages 1–14.
- Bentley, J. L. (1975). Multidimensional binary search trees used for associative searching. *Communications of the ACM*, 18(9):509–517.
- Blei, D. M., Kucukelbir, A., and McAuliffe, J. D. (2017). Variational inference: A review for statisticians. *Journal of the American statistical Association*, 112(518):859–877.
- Breheny, P. and Breheny, M. P. (2021). Package ‘nevrreg’.
- Bürkner, P.-C., Gabry, J., and Vehtari, A. (2021). Efficient leave-one-out cross-validation for bayesian non-factorized normal and student-t models. *Computational Statistics*, 36(2):1243–1261.
- Burt, D., Rasmussen, C. E., and Van Der Wilk, M. (2019). Rates of convergence for sparse variational gaussian process regression. In *International Conference on Machine Learning*, pages 862–871. PMLR.
- Carbonetto, P. and Stephens, M. (2012). Scalable variational inference for bayesian variable selection in regression, and its accuracy in genetic association studies. *Bayesian analysis*, 7(1):73–108.
- Chen, H., Zheng, L., Al Kontar, R., and Raskutti, G. (2020). Stochastic gradient descent in correlated settings: A study on gaussian processes. *Advances in Neural Information Processing Systems*, 33.
- Chicco, D. and Jurman, G. (2020). The advantages of the matthews correlation coefficient (mcc) over f1 score and accuracy in binary classification evaluation. *BMC genomics*, 21(1):1–13.
- Dai, Z., Hensman, J., and Lawrence, N. (2015). Spike and slab gaussian process latent variable models. *arXiv preprint arXiv:1505.02434*.
- Gardner, J. R., Pleiss, G., Bindel, D., Weinberger, K. Q., and Wilson, A. G. (2018). Gpytorch: Black-box matrix-matrix gaussian process inference with gpu acceleration. *arXiv preprint arXiv:1809.11165*.
- Gelman, A., Hwang, J., and Vehtari, A. (2014). Understanding predictive information criteria for bayesian models. *Statistics and computing*, 24(6):997–1016.
- George, E. I. and McCulloch, R. E. (1997). Approaches for bayesian variable selection. *Statistica sinica*, pages 339–373.
- Hensman, J., Fusi, N., and Lawrence, N. D. (2013). Gaussian processes for big data. *arXiv preprint arXiv:1309.6835*.
- Huang, J., Ma, S., Xie, H., and Zhang, C.-H. (2009). A group bridge approach for variable selection. *Biometrika*, 96(2):339–355.
- Ishwaran, H. and Rao, J. S. (2005). Spike and slab variable selection: frequentist and bayesian strategies. *The Annals of Statistics*, 33(2):730–773.
- Jankowiak, M. and Pleiss, G. (2021). Scalable cross validation losses for gaussian process models. *arXiv preprint arXiv:2105.11535*.
- Kingma, D. P. and Ba, J. (2014). Adam: A method for stochastic optimization. *arXiv preprint arXiv:1412.6980*.
- Kingma, D. P. and Welling, M. (2013). Auto-encoding variational bayes. *arXiv preprint arXiv:1312.6114*.
- Linkletter, C., Bingham, D., Hengartner, N., Higdon, D., and Ye, K. Q. (2006). Variable selection for gaussian process models in computer experiments. *Technometrics*, 48(4):478–490.
- Liu, R., Regier, J., Tripuraneni, N., Jordan, M., and McAuliffe, J. (2019). Rao-blackwellized stochastic gradients for discrete distributions. In *International Conference on Machine Learning*, pages 4023–4031. PMLR.
- Louizos, C., Ullrich, K., and Welling, M. (2017). Bayesian compression for deep learning. *arXiv preprint arXiv:1705.08665*.
- MacKay, D. J. et al. (1998). Introduction to gaussian processes. *NATO ASI series F computer and systems sciences*, 168:133–166.
- Matthews, B. W. (1975). Comparison of the predicted and observed secondary structure of t4 phage lysozyme. *Biochimica et Biophysica Acta (BBA)-Protein Structure*, 405(2):442–451.
- Mitchell, T. J. and Beauchamp, J. J. (1988). Bayesian variable selection in linear regression. *Journal of the american statistical association*, 83(404):1023–1032.
- Mohamed, S., Rosca, M., Figurnov, M., and Mnih, A. (2020). Monte carlo gradient estimation in machine learning. *J. Mach. Learn. Res.*, 21(132):1–62.
- Mohammed, R. O. and Cawley, G. C. (2017). Overfitting in model selection with gaussian process regression. In *International Conference on Machine Learning and Data Mining in Pattern Recognition*, pages 192–205. Springer.
- Narisetty, N. N. and He, X. (2014). Bayesian variable selection with shrinking and diffusing priors. *The Annals of Statistics*, 42(2):789–817.

-
- Ober, S. W., Rasmussen, C. E., and van der Wilk, M. (2021). The promises and pitfalls of deep kernel learning. *arXiv preprint arXiv:2102.12108*.
- Omohundro, S. M. (1989). *Five balltree construction algorithms*. International Computer Science Institute Berkeley.
- Paananen, T., Piironen, J., Andersen, M. R., and Vehtari, A. (2019). Variable selection for gaussian processes via sensitivity analysis of the posterior predictive distribution. In *The 22nd International Conference on Artificial Intelligence and Statistics*, pages 1743–1752. PMLR.
- Qamar, S. and Tokdar, S. T. (2014). Additive gaussian process regression. *arXiv preprint arXiv:1411.7009*.
- Ranganath, R., Gerrish, S., and Blei, D. (2014). Black box variational inference. In *Artificial intelligence and statistics*, pages 814–822. PMLR.
- Rasmussen, C. E. and Williams, C. K. (2006). Rasmussen and christopher ki williams. gaussian processes for machine learning. *MIT Press*, 211:212.
- Salimans, T. and Knowles, D. A. (2014). On using control variates with stochastic approximation for variational bayes and its connection to stochastic linear regression. *arXiv preprint arXiv:1401.1022*.
- Savitsky, T., Vannucci, M., and Sha, N. (2011). Variable selection for nonparametric gaussian process priors: Models and computational strategies. *Statistical science: a review journal of the Institute of Mathematical Statistics*, 26(1):130.
- Shahriari, B., Swersky, K., Wang, Z., Adams, R. P., and De Freitas, N. (2015). Taking the human out of the loop: A review of bayesian optimization. *Proceedings of the IEEE*, 104(1):148–175.
- Smith, S. L., Dherin, B., Barrett, D. G., and De, S. (2021). On the origin of implicit regularization in stochastic gradient descent. *arXiv preprint arXiv:2101.12176*.
- Tibshirani, R. (1996). Regression shrinkage and selection via the lasso. *Journal of the Royal Statistical Society: Series B (Methodological)*, 58(1):267–288.
- Titsias, M. (2009). Variational learning of inducing variables in sparse gaussian processes. In *Artificial intelligence and statistics*, pages 567–574. PMLR.
- Wang, K., Pleiss, G., Gardner, J., Tyree, S., Weinberger, K. Q., and Wilson, A. G. (2019). Exact gaussian processes on a million data points. *Advances in Neural Information Processing Systems*, 32:14648–14659.
- Wilson, A. G., Hu, Z., Salakhutdinov, R., and Xing, E. P. (2016). Deep kernel learning. In *Artificial intelligence and statistics*, pages 370–378. PMLR.
- Yao, Y., Vehtari, A., Simpson, D., and Gelman, A. (2018). Using stacking to average bayesian predictive distributions (with discussion). *Bayesian Analysis*, 13(3):917–1007.
- Zhang, C.-H. (2010). Nearly unbiased variable selection under minimax concave penalty. *The Annals of statistics*, 38(2):894–942.

7 Mathematical appendix

7.1 Kernel parameterisation

In this work we treat the inverse lengthscales of the kernel as being unconstrained in their parameterisation: $\boldsymbol{\theta} \in \mathbb{R}^d$. We note that although it is typical for inverse lengthscales to be strictly positive $\boldsymbol{\theta} \in \mathbb{R}_{>0}^d$, most kernel functions are invariant to the sign of θ_j for standard parameterisations. For example any stationary kernel function of the form given in eq. 1 in the main text (e.g. squared exponential, Matérn, Cauchy) is a function $g_{\mathbf{x}, \mathbf{x}'}(\theta_1^2, \dots, \theta_d^2)$. The linear kernel, polynomial kernel and periodic wrappers on anisotropic stationary kernels are also invariant to $\text{sign}(\theta_j)$. For any kernel where this invariance does not hold our procedure reparameterises the kernel in terms of $\boldsymbol{\theta} = \sqrt{\boldsymbol{\theta}}$. Thus initial use of a Mean-Field Gaussian posterior approximation $q_\psi(\boldsymbol{\theta}) = \prod_{j=1}^d \mathcal{N}(\theta_j | \mu_j, \sigma_j^2)$ over the inverse lengthscales is appropriate. Thus, any plots of posterior means $\{\mu_j\}_{j=1}^d$ using our method (the SSVGP) in the main text and this Appendix plot $\{|\mu_j|\}_{j=1}^d$.

7.2 SSVGP a-CAVI algorithm

Here we derive the mathematical form of the reparameterisation gradient approximations of the evidence lower bound (ELBO) $\nabla_\psi \hat{\mathcal{F}}$, $\nabla_\alpha \hat{\mathcal{F}}$ and fixed point updates for variational parameters $\boldsymbol{\lambda}, \boldsymbol{\xi}$ and in a-CAVI algorithm 1. We derive these for the case that $q_\psi(\boldsymbol{\theta})$ Mean-Field Gaussian, and discuss simplifications to this when the zero-temperature posterior restriction is used (i.e. in our main/final method).

7.2.1 ELBO gradients

We first derive expressions 5 and 6 in the main text for $\nabla_\psi \hat{\mathcal{F}}$ and $\nabla_\phi \hat{\mathcal{F}}$ respectively. We start with expression 2 in the main text for the evidence lower bound:

$$\mathcal{F} = \langle \log p_\phi(\mathbf{y}|\boldsymbol{\theta}) \rangle_{q_\psi(\boldsymbol{\theta})} - KL[q_\psi(\boldsymbol{\theta})q(\boldsymbol{\gamma})q(\boldsymbol{\pi})||p(\boldsymbol{\theta}, \boldsymbol{\gamma}, \boldsymbol{\pi})] \quad (13)$$

Taking gradients wrt. $\boldsymbol{\psi}$ we have:

$$\nabla_\psi \mathcal{F} = \nabla_\psi \langle \log p_\phi(\mathbf{y}|\boldsymbol{\theta}) \rangle_{q_\psi(\boldsymbol{\theta})} - \nabla_\psi KL[q_\psi(\boldsymbol{\theta})q(\boldsymbol{\gamma})q(\boldsymbol{\pi})||p(\boldsymbol{\theta}, \boldsymbol{\gamma}, \boldsymbol{\pi})] \quad (14)$$

The first term involves the gradient of an expectation of both (i) a log-determinant and (ii) inverse of the gram matrix $\tilde{K}_{XX} = K_{XX} + \sigma^2 I$. This is intractable to compute for most kernel functions, and thus needs to be approximated. We use the reparameterisation trick (Kingma and Welling, 2013) for this. The KL gradient however is exactly tractable.

For the reparameterisation trick to apply, $q_\psi(\boldsymbol{\theta})$ must be parameterised such that $\boldsymbol{\theta} = \mathcal{T}_\psi(\boldsymbol{\epsilon})$ and $\boldsymbol{\epsilon} \sim q(\boldsymbol{\epsilon})$. Here $\mathcal{T}_\psi(\cdot)$ is a transformation differentiable in $(\boldsymbol{\psi}, \boldsymbol{\epsilon})$, and $q(\boldsymbol{\epsilon})$ is a base distribution that does not depend on $\boldsymbol{\psi}$. In this case, using the law of the unconscious statistician and the chain rule we have the following:

$$\nabla_\psi \langle \log p_\phi(\mathbf{y}|\boldsymbol{\theta}) \rangle_{q_\psi(\boldsymbol{\theta})} = \nabla_\psi \int q_\psi(\boldsymbol{\theta}) \log p_\phi(\mathbf{y}|\boldsymbol{\theta}) d\boldsymbol{\theta} \quad (15)$$

$$= \nabla_\psi \int q(\boldsymbol{\epsilon}) \log p_\phi(\mathbf{y}|\boldsymbol{\theta}) \Big|_{\boldsymbol{\theta}=\mathcal{T}_\psi(\boldsymbol{\epsilon})} d\boldsymbol{\epsilon} \quad (16)$$

$$= \int q(\boldsymbol{\epsilon}) \nabla_\theta \log p_\phi(\mathbf{y}|\boldsymbol{\theta}) \Big|_{\boldsymbol{\theta}=\mathcal{T}_\psi(\boldsymbol{\epsilon})} \nabla_\psi \mathcal{T}_\psi(\boldsymbol{\epsilon}) d\boldsymbol{\epsilon} \quad (17)$$

$$= \langle \log p_\phi(\mathbf{y}|\boldsymbol{\theta}) \nabla_\psi \mathcal{T}_\psi(\boldsymbol{\epsilon}) \rangle_{q(\boldsymbol{\epsilon})} \quad (18)$$

Thus, given S Monte Carlo samples $\boldsymbol{\epsilon}^{(1:S)} \sim q(\boldsymbol{\epsilon})$ our unbiased approximation to $\nabla_\psi \mathcal{F}$ is:

$$\hat{\nabla}_\psi \mathcal{F} = \frac{1}{S} \sum_{s=1}^S \left(\nabla_\theta \log p_\phi(\mathbf{y}|\boldsymbol{\theta}) \Big|_{\boldsymbol{\theta}=\mathcal{T}_\psi(\boldsymbol{\epsilon}^{(s)})} \nabla_\psi \mathcal{T}_\psi(\boldsymbol{\epsilon}^{(s)}) \right) - \nabla_\psi KL[q_\psi(\boldsymbol{\theta})q(\boldsymbol{\gamma})||p(\boldsymbol{\theta}|\boldsymbol{\gamma})] \quad (19)$$

Note here that we have used that $\nabla_\psi KL[q_\psi(\boldsymbol{\theta})q(\boldsymbol{\gamma})q(\boldsymbol{\pi})||p(\boldsymbol{\theta}, \boldsymbol{\gamma}, \boldsymbol{\pi})] = \nabla_\psi KL[q_\psi(\boldsymbol{\theta})q(\boldsymbol{\gamma})||p(\boldsymbol{\theta}|\boldsymbol{\gamma})]$. Note for Mean-Field Gaussian $q_\psi(\boldsymbol{\theta}) = \mathcal{N}(\boldsymbol{\theta}|\boldsymbol{\mu}, \text{Diag}(\sigma_1^2, \dots, \sigma_d^2))$ we set $\mathcal{T}_\psi(\boldsymbol{\epsilon}) = \boldsymbol{\sigma} \odot \boldsymbol{\epsilon} + \boldsymbol{\mu}$ and $q(\boldsymbol{\epsilon}) = \mathcal{N}(\mathbf{0}, I)$.

The equivalent gradient approximation for $\hat{\nabla}_\phi \mathcal{F}$ given in the main text is trivial to derive:

$$\hat{\nabla}_\phi \mathcal{F} = \nabla_\phi \langle \log p_\phi(\mathbf{y}|\boldsymbol{\theta}) \rangle_{q_\psi(\boldsymbol{\theta})} \quad (20)$$

$$= \int \nabla_\phi \log p_\phi(\mathbf{y}|\boldsymbol{\theta}) q_\psi(\boldsymbol{\theta}) d\boldsymbol{\theta} \quad (21)$$

$$\hat{\nabla}_\phi \mathcal{F} \approx \frac{1}{S} \sum_{s=1}^S \nabla_\phi \log p_\phi(\mathbf{y}|\boldsymbol{\theta}^{(s)}) : \boldsymbol{\theta}^{(s)} \sim q_\psi(\boldsymbol{\theta}^{(s)}) \quad (22)$$

We now derive the closed forms of the main components in the gradient approximations above. Note that when $\log p_\phi(\mathbf{y}|\boldsymbol{\theta}) = \log \mathcal{N}(\mathbf{y}|\mathbf{0}, \tilde{K}_{XX})$ with $n \times n$ gram matrix \tilde{K}_{XX} comprised of covariance kernel function evaluations and the additive noise term $[\tilde{K}_{XX}]_{ij} = k_{\boldsymbol{\theta}, \tau}(\mathbf{x}_i, \mathbf{x}_j) + \delta_0(i = j)\sigma^2$, then using standard results derived in [Rasmussen and Williams \(2006\)](#) we have:

$$\nabla_{\theta_j} \log_\phi p(\mathbf{y}|\boldsymbol{\theta}) = \text{Tr} \left[(\boldsymbol{\alpha} \boldsymbol{\alpha}^T - \tilde{K}_{XX}^{-1}) \frac{d\tilde{K}_{XX}}{d\theta_j} \right] : \boldsymbol{\alpha} = \tilde{K}_{XX}^{-1} \mathbf{y} \quad (23)$$

$$\nabla_{\phi_j} \log_\phi p(\mathbf{y}|\boldsymbol{\theta}) = \text{Tr} \left[(\boldsymbol{\alpha} \boldsymbol{\alpha}^T - \tilde{K}_{XX}^{-1}) \frac{d\tilde{K}_{XX}}{d\phi_j} \right] : \boldsymbol{\alpha} = \tilde{K}_{XX}^{-1} \mathbf{y} \quad (24)$$

Meanwhile, the closed form for the gradient of the KL term wrt. $\boldsymbol{\psi}$ is:

$$\nabla_\psi KL[q_\psi(\boldsymbol{\theta})q(\gamma)||p(\boldsymbol{\theta}|\gamma)] = \nabla_\psi \int \sum_\gamma q_\psi(\boldsymbol{\theta})q(\gamma) \log p(\boldsymbol{\theta}|\gamma) d\boldsymbol{\theta} + \nabla_\psi H[q_\psi(\boldsymbol{\theta})] \quad (25)$$

$$= \nabla_\psi \sum_{j=1}^d \left[\langle \gamma_j \rangle_{q(\gamma_j)} \langle \log \mathcal{N}(\theta_j|0, (cv)^{-1}) \rangle_{q_{\psi_j}(\theta_j)} \right. \\ \left. + (1 - \langle \gamma_j \rangle_{q(\gamma_j)}) \langle \log \mathcal{N}(\theta_j|0, v^{-1}) \rangle_{q_{\psi_j}(\theta_j)} \right] + \nabla_\psi H[q_\psi(\boldsymbol{\theta})] \quad (26)$$

$$= -\frac{1}{2} \nabla_\psi \sum_{j=1}^d \left[\lambda_j cv \langle \theta_j^2 \rangle_{q_\psi(\boldsymbol{\theta})} + (1 - \lambda_j) v \langle \theta_j^2 \rangle_{q_\psi(\boldsymbol{\theta})} \right] + \nabla_\psi H[q_\psi(\boldsymbol{\theta})] \quad (27)$$

$$= -\frac{v}{2} \nabla_\psi \sum_{j=1}^d (\lambda_j c + 1 - \lambda_j) \langle \theta_j^2 \rangle_{q_\psi(\boldsymbol{\theta})} + \nabla_\psi H[q_\psi(\boldsymbol{\theta})] \quad (28)$$

Note that $H[q_\psi(\boldsymbol{\theta})]$ is the Shannon entropy of $q_\psi(\boldsymbol{\theta})$. Substituting in $q_\psi(\boldsymbol{\theta}) = \prod_{j=1}^d \mathcal{N}(\theta_j|\mu_j, \sigma_j^2)$, and using standard Gaussian algebra we get the equations in the main text:

$$\nabla_\mu KL[q_\psi(\boldsymbol{\theta})q(\gamma)||p(\boldsymbol{\theta}|\gamma)] = -v(\boldsymbol{\lambda}c + \mathbf{1} - \boldsymbol{\lambda}) \odot \boldsymbol{\mu} \quad (29)$$

$$\nabla_\sigma KL[q_\psi(\boldsymbol{\theta})q(\gamma)||p(\boldsymbol{\theta}|\gamma)] = -v(\boldsymbol{\lambda}c + \mathbf{1} - \boldsymbol{\lambda}) \odot \boldsymbol{\sigma} + \boldsymbol{\sigma}^{-1} \quad (30)$$

Here we can see the regularising effect that the KL term has on the posterior over the inverse lengthscales. The effect is stronger for the posterior means as the Gaussian entropy term explodes as $\boldsymbol{\sigma} \rightarrow 0$, preventing neighbourhood zero values for the posterior variances.

Under the zero-temperature restriction ($q_\psi(\boldsymbol{\theta}) = \prod_{j=1}^d \delta_{\mu_j}(\theta_j)$) the gradient approximations are unchanged, except now the approximation is exact for a single sample from the point mass ($\boldsymbol{\theta}^{(s)} = \boldsymbol{\mu}$), and $\boldsymbol{\psi} = \boldsymbol{\mu}$.

7.2.2 Fixed points

Starting with the standard CAVI update expression in Blei et al. (2017), the update for $q(\gamma)$ is given by:

$$\begin{aligned} q(\gamma) &\propto \exp \left\{ \langle \log p(\boldsymbol{\theta}, \gamma | \pi) \rangle_{q_{\psi}(\boldsymbol{\theta})q(\pi)} \right\} \\ &\propto \prod_{j=1}^d \exp \left\{ \gamma_j \langle \log \mathcal{N}(\theta_j | 0, (cv)^{-1}) \rangle_{q_{\psi_j}(\theta_j)} + (1 - \gamma_j) \langle \log \mathcal{N}(\theta_j | 0, v^{-1}) \rangle_{q_{\psi_j}(\theta_j)} \right. \\ &\quad \left. + \gamma_j \langle \log \pi \rangle_{q(\pi)} + (1 - \gamma_j) \langle \log(1 - \pi) \rangle_{q(\pi)} \right\} \end{aligned} \quad (31)$$

Passing over the Gaussian expectations, we have due to the factorisation of the RHS that:

$$q(\gamma_j = 1) = \lambda_j \propto c^{\frac{1}{2}} e^{-\frac{1}{2}cv \langle \theta_j^2 \rangle_{q_{\psi_j}(\theta_j)} + \langle \log \pi \rangle_{q(\pi)}} \quad (32)$$

$$q(\gamma_j = 0) \propto e^{-\frac{1}{2}v \langle \theta_j^2 \rangle_{q_{\psi_j}(\theta_j)} + \langle \log(1 - \pi) \rangle_{q(\pi)}} \quad (33)$$

After renormalisation we arrive at the update used in a-CAVI algorithm 1:

$$\lambda_j = \left(1 + \left(\frac{1}{c} \right)^{\frac{1}{2}} e^{-\frac{1}{2} \langle \theta_j^2 \rangle_{q_{\psi_j}(\theta_j)} v(1-c) + \langle \log \left(\frac{1-\pi}{\pi} \right) \rangle_{q(\pi)}} \right)^{-1} \quad (34)$$

Where note that $\langle \boldsymbol{\theta} \odot \boldsymbol{\theta} \rangle_{q_{\psi}(\boldsymbol{\theta})} = \boldsymbol{\mu} \odot \boldsymbol{\mu} + \boldsymbol{\sigma} \odot \boldsymbol{\sigma}$ using standard properties of multivariate Gaussians. Similarly, since $q(\pi) = \text{Beta}(\pi | \xi_a, \xi_b)$ (see below), we have using the properties of the Beta distribution that for digamma function $\tilde{\psi}_0(\cdot)$:

$$\left\langle \log \left(\frac{1 - \pi}{\pi} \right) \right\rangle_{q(\pi)} = \tilde{\psi}_0(\xi_b) - \tilde{\psi}_0(\xi_a) \quad (35)$$

For the CAVI update for $q(\pi)$ we have:

$$\begin{aligned} q(\pi) &\propto \exp \left\{ \langle \log p(\gamma, \pi) \rangle_{q(\gamma)} \right\} \\ &\propto \exp \left\{ \left(a - 1 + \sum_{j=1}^d \langle \gamma_j \rangle_{q(\gamma_j)} \right) \log(\pi) + \left(b - 1 + d - \sum_{j=1}^d \langle \gamma_j \rangle_{q(\gamma_j)} \right) \log(1 - \pi) \right\} \\ &\propto \text{Beta} \left(\pi | a + \sum_{j=1}^d \langle \gamma_j \rangle_{q(\gamma_j)}, b + d - \sum_{j=1}^d \langle \gamma_j \rangle_{q(\gamma_j)} \right) \\ &\propto \text{Beta}(\pi | a + d\bar{\lambda}, b + d(1 - \bar{\lambda})) \quad : \quad \bar{\lambda} = \frac{1}{d} \sum_{j=1}^d \lambda \end{aligned} \quad (36)$$

Therefore $\boldsymbol{\xi} = (\xi_a, \xi_b) = \left(a + \sum_{j=1}^d \langle \gamma_j \rangle_{q(\gamma_j)}, b + d - \sum_{j=1}^d \langle \gamma_j \rangle_{q(\gamma_j)} \right)$ and the expected sufficient statistic $\langle \log \frac{1-\pi}{\pi} \rangle_{q(\pi)}$ is given by expression 35 above.

7.3 SSVGP leave-one-out log predictive density (LOO-LPD)

Here we briefly derive the mathematical form of the leave-one-out log predictive density under a given model \mathcal{M}_k in the BMA ensemble under the zero-temperature posterior. The easiest way to do this is to note that model \mathcal{M}_k is defined by parameters $\boldsymbol{\nu}_k = (\boldsymbol{\mu}_k, \boldsymbol{\phi}_k, a, b, c, v_k)$. Note here we treat inverse lengthscales $\boldsymbol{\theta}$ as fixed at posterior means $\boldsymbol{\mu}_k$, since this is equivalent to using a zero-temperature posterior $q_{\psi}(\boldsymbol{\theta}) = \prod_{j=1}^d \delta_{\mu_j}(\theta_j)$. Thus, since kernel parameters are fixed the LOO-LPD for model k is simply that of a standard GP evaluated at $(\boldsymbol{\theta} = \boldsymbol{\mu}_k, \boldsymbol{\phi} = \boldsymbol{\phi}_k)$

(Rasmussen and Williams, 2006) (note we assume a zero mean GP prior as typical):

$$\sum_{i=1}^n \log p(y_i | \mathcal{D}_{-i}, \mathbf{x}_i, \mathcal{M}_k) = \sum_{i=1}^n \log p_{\phi_k, \theta_k}(y_i | \mathcal{D}_{-i}, \mathbf{x}_i) \quad (37)$$

$$= \sum_{i=1}^n \log \mathcal{N}(y_i | \mu_i, \sigma_i^2) \quad (38)$$

$$\mu_i = \mathbf{k}_{X_{-i}}(\mathbf{x}_i)^T (K_{X_{-i}X_{-i}} + \sigma^2 I)^{-1} \mathbf{y}_{-i} \quad (39)$$

$$\sigma_i^2 = k_{\mu_k, \tau_k}(\mathbf{x}_i, \mathbf{x}_i) - \mathbf{k}_{X_{-i}}(\mathbf{x}_i)^T (K_{X_{-i}X_{-i}} + \sigma^2 I)^{-1} \mathbf{k}_{X_{-i}}(\mathbf{x}_i) + \sigma^2 \quad (40)$$

Here $K_{X_{-i}X_{-i}}$ is the $(n-1) \times (n-1)$ gram matrix of training points when removing (y_i, \mathbf{x}_i) , and $\mathbf{k}_{X_{-i}}(\mathbf{x}_i)$ is an $n-1$ dimensional vector of kernel function evaluations between \mathbf{x}_i and all other training points. As discussed in the main text we use the algorithm in Bürkner et al. (2021) in small- n scenarios ($\mathcal{O}(n^3)$ complexity) and the nearest neighbour truncation algorithm in Jankowiak and Pleiss (2021) in large- n scenarios ($\mathcal{O}(nf(n)d)$ complexity with $f(n) \in [\log(n), n]$). In some circumstances we add a small regularisation term of $0 < \kappa \ll 1$ to the posterior variances small- n scenarios to prevent outliers from blowing up the negative LOO-LPD. We only find it necessary to do this in the toy example (setting $\kappa = 0.1$), but in all main experiments performance is robust to $\kappa \in [0, 1]$.

7.4 SSVGP predictive distribution

Here we derive the closed form predictive moments given by the predictive distribution approximations in eq. 8 and 12 in the main text. Since both distributions are discrete mixtures of standard GP posterior predictives with the k^{th} component parameterised by inverse lengthscales θ_k kernel scale and noise parameters ϕ_k , we derive the moments for this distributional family. However note that for eq. 8 in the main text (i.e. the SSVGP posterior predictive with Mean-Field Gaussian $q_\psi(\theta)$ and fixed v), the distribution is an approximation to the true predictive posterior, and thus the predictive covariance derived below is a biased but consistent estimator (it contains a product of approximate expectations).

We define the distributional family we work with as follows:

$$p(\mathbf{y}_* | X_*, \mathcal{D}) = \sum_{k=1}^K p_{\theta_k, \phi_k}(\mathbf{y}_* | X_*, \mathcal{D}) w_k \quad (41)$$

Here $\{w_k\}_{k=1}^K$ are the mixture weights and $p_{\theta_k, \phi_k}(\mathbf{y}_* | X_*, \mathcal{D})$ is a standard GP posterior predictive given (θ_k, ϕ_k) . In this case, the posterior predictive posterior mean is computed as:

$$\begin{aligned} \mathbf{m}(X_*) &= \mathbb{E}[\mathbf{y}_* | X_*, \mathcal{D}] = \int \mathbf{y}_* \sum_{k=1}^K p_{\theta_k, \phi_k}(\mathbf{y}_* | X_*, \mathcal{D}) w_k d\mathbf{y}_* \\ &= \sum_{k=1}^K w_k \int \mathbf{y}_* p_{\theta_k, \phi_k}(\mathbf{y}_* | X_*, \mathcal{D}) d\mathbf{y}_* \\ &= \sum_{k=1}^K w_k \boldsymbol{\xi}_{\theta_k, \phi_k}(X_*) \end{aligned} \quad (42)$$

Where $\boldsymbol{\xi}_{\theta_k, \phi_k}(X_*) = \mathbb{E}_{p_{\theta_k, \phi_k}(\mathbf{y}_* | X_*, \mathcal{D})}[\mathbf{y}_*]$ is the mean of standard GP posterior predictive component $p_{\theta_k, \phi_k}(\mathbf{y}_* | X_*, \theta_k, \mathcal{D})$ (see Rasmussen and Williams (2006) for details).

Similarly, using the definition of covariance: $\mathbb{V}[\mathbf{x}] = \mathbb{E}[\mathbf{x}\mathbf{x}^T] - \mathbb{E}[\mathbf{x}]\mathbb{E}[\mathbf{x}]^T$, the posterior covariance is given as:

$$\begin{aligned} \mathbf{V}(X_*) &= \mathbb{V}[\mathbf{y}_* | X_*, \mathcal{D}] = \sum_{k=1}^K w_k \int \mathbf{y}_* \mathbf{y}_*^T p_{\theta_k, \phi_k}(\mathbf{y}_* | X_*, \mathcal{D}) d\mathbf{y}_* - \mathbf{m}(X_*) \mathbf{m}(X_*)^T \\ &= \sum_{k=1}^K w_k (\boldsymbol{\Sigma}_{\theta_k, \phi_k}(X_*) + \boldsymbol{\xi}_{\theta_k, \phi_k}(X_*) \boldsymbol{\xi}_{\theta_k, \phi_k}(X_*)^T) - \mathbf{m}(X_*) \mathbf{m}(X_*)^T \end{aligned} \quad (43)$$

Where $\Sigma_{\theta_k, \phi_k}(X_*) = \text{Var}_{p_{\theta_k, \phi_k}(\mathbf{y}_*|X_*, \mathcal{D})}[\mathbf{y}_*]$ is the covariance of standard GP posterior predictive component $p_{\theta_k, \phi_k}(\mathbf{y}_*|X_*, \theta_k, \mathcal{D})$ (see [Rasmussen and Williams \(2006\)](#) for details)

7.5 SSVGP posterior point of intersection (PPI)

Here we derive equation 11 in the main text for the posterior point of intersection (PPI). The PPI is given by $\hat{\theta} = \sqrt{\langle \theta^2 \rangle_{q_{\psi_j}(\theta)}}$ such that $q(\gamma = 1) = q(\gamma = 0) = \frac{1}{2}$. To derive the expression we substitute $\lambda = \frac{1}{2}$ into the optimal CAVI update for λ given by equation 34:

$$\frac{1}{2} = \left(1 + \left(\frac{1}{c} \right)^{\frac{1}{2}} e^{-\frac{1}{2} \langle \theta_j^2 \rangle_{q_{\psi_j}(\theta_j)} v(1-c) + \langle \log \left(\frac{1-\pi}{\pi} \right) \rangle_{q(\pi)}} \right)^{-1} \quad (44)$$

Re-arranging terms we get:

$$1 = \left(\frac{1}{c} \right)^{\frac{1}{2}} e^{-\frac{1}{2} \langle \theta_j^2 \rangle_{q_{\psi_j}(\theta_j)} v(1-c) + \langle \log \left(\frac{1-\pi}{\pi} \right) \rangle_{q(\pi)}} \quad (45)$$

$$0 = \frac{1}{2} \log \left(\frac{1}{c} \right) - \frac{1}{2} \langle \theta_j^2 \rangle_{q_{\psi_j}(\theta_j)} v(1-c) + \left\langle \log \left(\frac{1-\pi}{\pi} \right) \right\rangle_{q(\pi)} \quad (46)$$

Taking the expected sufficient statistic of θ_j to the LHS and simplifying we get:

$$\langle \theta_j^2 \rangle_{q_{\psi_j}(\theta_j)} v(1-c) = \log \left(\frac{1}{c} \right) + 2 \left\langle \log \left(\frac{1-\pi}{\pi} \right) \right\rangle_{q(\pi)} \quad (47)$$

Thus finally we arrive at the equation in the main text:

$$\sqrt{\langle \theta_j^2 \rangle_{q_{\psi_j}(\theta_j)}} = \hat{\theta} = \sqrt{\frac{\log \left(\frac{1}{c} \right) + 2 \langle \log \left(\frac{1-\pi}{\pi} \right) \rangle_{q(\pi)}}{v(1-c)}} \quad (48)$$

7.6 SSVGP fixed variable inclusion cost

In Section 4 we discuss that the evidence lower bound has a fixed variable ‘inclusion cost’ of order $\log(\frac{1}{c})$, making it unideal for model selection as c can heavily impact the degree of preference for sparse models. Here we derive the source of this inclusion cost. Starting from the KL regularisation term of the evidence lower bound, note that under an arbitrary inverse lengthscale posterior $q_{\psi}(\theta)$, if we retain only the terms that include $\{\langle \theta_j^2 \rangle_{q_{\psi_j}(\theta_j)}\}_{j=1}^d$ and $\{\lambda_j\}_{j=1}^d$, we are left with:

$$\begin{aligned} -KL[q_{\psi}(\theta)q(\gamma)q(\pi)||p(\theta, \gamma, \pi)] &= \frac{1}{2} \sum_{j=1}^d \lambda_j \log(c) - \frac{v}{2} \sum_{j=1}^d \langle \theta_j^2 \rangle_{q_{\psi_j}(\theta_j)} (\lambda_j c + 1 - \lambda_j) \\ &\quad + \sum_{j=1}^d \lambda_j \left\langle \log \left(\frac{\pi}{\lambda_j} \right) \right\rangle_{q(\pi)} + \sum_{j=1}^d (1 - \lambda_j) \left\langle \log \left(\frac{1-\pi}{1-\lambda_j} \right) \right\rangle_{q(\pi)} \\ &\quad + \text{const. wrt. } (\{\langle \theta_j^2 \rangle_{q_{\psi_j}(\theta_j)}, \lambda_j\}_{j=1}^d) \end{aligned} \quad (49)$$

The contribution of variable j to these components of the KL is given by:

$$\zeta_j = \lambda_j \frac{1}{2} \log(c) - \frac{v}{2} \langle \theta_j^2 \rangle_{q_{\psi_j}(\theta_j)} (\lambda_j c + 1 - \lambda_j) + \lambda_j \left\langle \log \left(\frac{\pi}{\lambda_j} \right) \right\rangle_{q(\pi)} + (1 - \lambda_j) \left\langle \log \left(\frac{1-\pi}{1-\lambda_j} \right) \right\rangle_{q(\pi)} \quad (50)$$

Clearly when moving from $\lambda_j : 0 \rightarrow 1$, there is a fixed inclusion cost from the first term of $\frac{1}{2} \log(\frac{1}{c})$. As a result the value of c can have a substantial effect on whether \mathcal{F} is higher when the average PIP is higher, which we find experimentally. This makes it challenging to use \mathcal{F} reliably to do discrete model selection or averaging.

7.7 Dirac spike with paired mean field (PMF) approximation

In Section 4 we also implement a spike and slab GP using a Dirac point mass at zero for the spike prior distribution, and the paired mean field variational approximation used in Dai et al. (2015) and Carbonetto and Stephens (2012):

$$q(\boldsymbol{\theta}|\boldsymbol{\gamma})q(\boldsymbol{\gamma}) = \prod_{d=1}^d [\mathcal{N}(\theta_j|\mu_j, \sigma_j^2)\lambda_j]^{\gamma_j} [\delta_0(\theta_j)(1 - \lambda_j)]^{1-\gamma_j} \quad (51)$$

This factorisation has the attractive property of retaining posterior dependence between the j^{th} inclusion variable γ_j and inverse lengthscale θ_j . However the cost of this dependency is that exact CAVI updates for $q(\boldsymbol{\gamma})$ are no longer tractable as it requires computing expectations of the likelihood term $\log p(\mathbf{y}|\boldsymbol{\theta})$, which are intractable for most kernel functions:

$$q(\gamma_j) \propto \exp(\langle \log p(\mathbf{y}|\boldsymbol{\theta}) \rangle_{q(\boldsymbol{\theta}|\boldsymbol{\gamma})} + \langle \log p(\theta_j, \gamma_j) \rangle_{q(\theta_j|\gamma_j)}) \quad (52)$$

Note that even if the expectations $\langle \log p(\mathbf{y}|\boldsymbol{\theta}) \rangle_{q(\boldsymbol{\theta}|\boldsymbol{\gamma})}$ could be computed for a setting of $\boldsymbol{\gamma}$, we would need to compute 2^{d-1} of these quantities. The complexity of this CAVI update would therefore be $\mathcal{O}(2^d n^3)$, which is computationally infeasible for large- n or even moderate d .

Our implementation therefore optimises $q(\boldsymbol{\theta}, \boldsymbol{\gamma})$ using stochastic gradient variational inference. We use score-gradients (aka BBVI (Ranganath et al., 2014)) to estimate $\nabla_{\boldsymbol{\lambda}} \mathcal{F}$ (since $\boldsymbol{\gamma}$ are non-differentiable) and reparameterisation gradients (aka repgrad (Kingma and Welling, 2013)) to estimate $\nabla_{\boldsymbol{\psi}} \mathcal{F}$:

$$\nabla_{\boldsymbol{\psi}} \mathcal{F} \approx \frac{1}{S_0} \sum_{s=1}^{S_0} \nabla_{\boldsymbol{\theta}} \log p(\mathbf{y}|\boldsymbol{\theta}^{(s)}) \Big|_{\boldsymbol{\theta}^{(s)} = \mathcal{T}_{\boldsymbol{\psi}}(\boldsymbol{\epsilon}^{(s)}, \mathbf{z}^{(s)})} \nabla_{\boldsymbol{\psi}} \mathcal{T}_{\boldsymbol{\psi}}(\boldsymbol{\epsilon}^{(s)}, \mathbf{z}^{(s)}) - \nabla_{\boldsymbol{\psi}} KL[q(\boldsymbol{\theta}|\boldsymbol{\gamma})q(\boldsymbol{\gamma})||p(\boldsymbol{\theta}, \boldsymbol{\gamma})] \quad (53)$$

$$\nabla_{\boldsymbol{\lambda}} \mathcal{F} \approx \frac{1}{S_1} \sum_{s=1}^{S_1} \left(\log p(\mathbf{y}|\boldsymbol{\theta}^{(s)}) \nabla_{\boldsymbol{\lambda}} \log q(\boldsymbol{\theta}^{(s)}) \right) \Big|_{\boldsymbol{\theta}^{(s)} = \mathcal{T}_{\boldsymbol{\psi}}(\boldsymbol{\epsilon}^{(s)}, \mathbf{z}^{(s)})} - \nabla_{\boldsymbol{\lambda}} KL[q(\boldsymbol{\theta}|\boldsymbol{\gamma})q(\boldsymbol{\gamma})||p(\boldsymbol{\theta}, \boldsymbol{\gamma})] \quad (54)$$

Note that now the differentiable transformation is $\mathcal{T}_{\boldsymbol{\psi}}(\boldsymbol{\epsilon}, \mathbf{z}) = \delta_{\mathbf{1}}(\mathbf{z} \leq \boldsymbol{\lambda}) \odot (\boldsymbol{\epsilon} \odot \boldsymbol{\sigma} + \boldsymbol{\mu})$, whereby $\mathbf{z} \sim \mathcal{U}[0, 1]^d$ and $\boldsymbol{\epsilon} \sim \mathcal{N}(\mathbf{0}, I)$ are drawn from the base distributions. Also note that the marginal distribution over inverse lengthscales is $q_{\boldsymbol{\psi}}(\boldsymbol{\theta}) = \prod_{j=1}^d [\lambda_j \mathcal{N}(\theta_j|\mu_j, \sigma_j^2) + (1 - \lambda_j) \delta_0(\theta_j)]$. In practice we reparameterise the model in terms of $\boldsymbol{\kappa} \in \mathbb{R}^d$ where $\boldsymbol{\lambda} = (\mathbf{1} - \exp(-\boldsymbol{\kappa}))^{-1}$ and optimise $\boldsymbol{\kappa}$. We set $S_0 = 1$ consistent with our a-CAVI algorithm, but set $S_1 \in \{10, 100\}$ (i.e. two implementations used) due to the much higher degree of score-gradient variance. We treat (π, v) as fixed parameters but pre-tune these to optimise performance for comparison against our SSVGP with the a-CAVI algorithm. See Appendix 2.1 for implementation details.

7.8 A mode seeking property of a-CAVI with implications for dropout

In this section we present and prove a ‘mode-seeking’ property of a-CAVI Algorithm 1 when $q_{\boldsymbol{\psi}}(\boldsymbol{\theta})$ is a zero-temperature distribution. We subsequently discuss how this property can be used to motivate the dropout pruning procedure we introduce in Section 4 of the main text. For simplicity our proof is for a 1d-input scenario but can be extended to multiple input dimensions.

The conditions required for this property to hold are strong and only apply under a simplification of the a-CAVI algorithm. However they mathematically formalise the notion that when the spike and slab parameter v is set large enough, small PIP values $\lambda \approx 0$ can result in the KL regularisation term dominating the likelihood term in the evidence lower bound and its gradients. In practice we find (μ, λ) both typically converge to near-zero values in these scenarios. In the proposition we go one step further by formalising conditions that guarantee a sequence of monotonically decreasing updates to $(|\mu|, \lambda)$ when running iterations of a simplified version of a-CAVI algorithm 1.

PROPOSITION 1 *Consider the spike and slab Gaussian process model defined in Section 3 of the main text where $\mathbf{y} \in \mathbb{R}^n$, $X \in \mathbb{R}^{n \times 1}$ is the dataset, $\theta \in \mathbb{R}^1$ is the inverse lengthscale, $\boldsymbol{\phi} = (\tau, \sigma^2) \in \mathbb{R}_{>0}^2$ are kernel scale*

¹See Appendix 7.1 for our explanation for the unconstrained parameterisation.

and noise parameters, $\gamma \in \{0, 1\}$ is the latent binary inclusion variable, $\pi \in [0, 1]$, and spike and slab prior is parameterised such that $(v, c) \in \mathbb{R}_{>0}^2$ with $0 < c \ll 1$. Let the a-CAVI algorithm be defined by the following simplifications. We use zero-temperature posterior $q_{\psi_j}(\theta) = \delta_{\mu}(\theta)$ such that $\theta = \mu$, let the prior inclusion probability π be fixed at $\pi_0 \in (0, 1)^2$ and fix $\phi = \hat{\phi}$. Now, assume the following conditions hold for some $\epsilon \in (0, 1)$:

$$v \geq \left(\frac{1}{1 - \epsilon} \right) \max_{\theta \in \Theta_{-0}} \left\{ \frac{\nabla_{\theta} \log p_{\hat{\phi}}(\mathbf{y}|\theta)}{\theta} \right\} \quad (55)$$

$$\eta_t \in \left(0, \left(v - \left\{ \frac{\nabla_{\theta} \log p_{\hat{\phi}}(\mathbf{y}|\theta)}{\theta} \right\} \Big|_{\theta=\mu_{(t)}} \right)^{-1} \right) \forall t \in [T], \forall T \in \mathbb{Z}_+ \quad (56)$$

$$|\mu_{(0)}| \leq \sqrt{\frac{2 \log \left(\frac{\epsilon(1-\pi_0)}{c^{\frac{1}{2}} \pi_0 (1-\epsilon)} \right)}{v(1-c)}} \quad (57)$$

Here $\{\eta_t\}_{t=0}^T > 0$ are the sequence of learning rates for the inverse lengthscale parameter, $\epsilon \in (0, 1)$ and $\mu_{(0)}$ is the inverse lengthscale posterior mean after the first set of gradient updates to $q(\theta)$. Then, $\forall t \in \mathbb{Z}_+$, we have that after t a-CAVI iterations of A1:

$$|\mu_{(t)}| < |\mu_{(t-1)}| \dots < |\mu_{(0)}| \quad (58)$$

$$\lambda_{(t)} < \lambda_{(t-1)} \dots < \lambda_{(0)} \quad (59)$$

PROOF:

We first demonstrate that if condition 61 is satisfied, then the initial CAVI update for λ (after recovering $\mu_{(0)}$) sets $\lambda_{(0)} \leq \epsilon$. This is easy to show since we can simply re-arrange expression 61 to get the following inequality:

$$\frac{1}{\epsilon} \leq 1 + c^{-\frac{1}{2}} e^{-\frac{1}{2} |\mu_{(0)}|^2 v(1-c)} \left(\frac{1 - \pi_0}{\pi_0} \right) \quad (60)$$

Now note the RHS is $\frac{1}{\lambda_{(0)}}$ when $\lambda_{(0)}$ is set using its CAVI update 34 under the restrictions of the a-CAVI algorithm in the proposition. Thus we clearly have $\lambda_{(0)} \leq \epsilon \in (0, 1)$.

We next show that if $\lambda_{(0)} \leq \epsilon$, then under 55 and the conditions of Proposition 1 we have that:

$$|\mu_{(1)}| = \left| \mu_{(0)} + \eta_0 \nabla_{\mu} \mathcal{F} \Big|_{\mu=\mu_{(0)}, \lambda=\lambda_{(0)}} \right| \leq |\mu_{(0)}| \quad (61)$$

Note \mathcal{F} is the evidence lower bound of the model as defined in the main text and Appendix 1. To show this, we start from condition 55 and denote $\nabla_{\theta} MLL = \nabla_{\theta} \log p_{\hat{\phi}}(\mathbf{y}|\theta)$ for convenience (MLL = marginal log likelihood). Thus we can re-write condition 55 as:

$$v(1 - \epsilon) \geq \frac{\nabla_{\theta} MLL}{\theta} \quad \forall \theta \in \Theta_{-0} \quad (62)$$

Now since $1 - \epsilon \leq 1 - \lambda_{(0)}$ and $v > 0$, $c > 0$, we have that:

$$v(1 - \lambda_{(0)}) + cv\lambda_{(0)} > v(1 - \epsilon) \geq \frac{\nabla_{\theta} MLL}{\theta} \quad \forall \theta \in \Theta_{-0} \quad (63)$$

²This can be simulated by setting Beta prior hyperparameters to $a = \tau$, $b = \tau \left(\frac{1}{\pi_0} - 1 \right)$ and letting $\tau \rightarrow \infty$.

Note the strict inequality arises since $\lambda_{(0)} > 0$. Simplifying the above expression, we get the following condition:

$$\frac{\nabla_{\theta} MLL}{\theta} - v(1 - \lambda_{(0)} + c\lambda_{(0)}) < 0 \quad \forall \theta \in \Theta_{-0} \quad (64)$$

Now we consider two case distinctions : (1) $\theta > 0$, (2) $\theta < 0$. In each case the above expression implies the following:

$$\nabla_{\theta} MLL - \theta v(1 - \lambda_{(0)} + c\lambda_{(0)}) < 0 \quad \forall \theta > 0 \quad (65)$$

$$\nabla_{\theta} MLL - \theta v(1 - \lambda_{(0)} + c\lambda_{(0)}) > 0 \quad \forall \theta < 0 \quad (66)$$

The left-hand-side is clearly equal to the gradient of the evidence lower bound $(\nabla_{\mu} \mathcal{F}|_{\mu=\theta, \lambda=\lambda_{(0)}})$ with respect to μ when $\mu = \theta$ and $\lambda = \lambda_{(0)}$ as derived in Appendix 1. Equations 65 and 66 therefore let us write:

$$\text{sign}(\nabla_{\mu} \mathcal{F}|_{\mu=\mu_{(0)}, \lambda=\lambda_{(0)}}) = -\text{sign}(\mu) \quad \forall \mu \neq 0 \quad (67)$$

By implication, we have that for any strictly positive learning rate η_0 :

$$\mu_{(0)} + \eta_0 \nabla_{\mu} \mathcal{F}|_{\mu=\mu_{(0)}, \lambda=\lambda_{(0)}} < \mu_{(0)} \quad \forall \mu_{(0)} > 0 \quad (68)$$

$$\mu_{(0)} + \eta_0 \nabla_{\mu} \mathcal{F}|_{\mu=\mu_{(0)}, \lambda=\lambda_{(0)}} > \mu_{(0)} \quad \forall \mu_{(0)} < 0 \quad (69)$$

Therefore, for condition 61 to hold, we simply require that:

$$\mu_{(1)} = \mu_{(0)} + \eta_0 \underbrace{\nabla_{\mu} \mathcal{F}|_{\mu=\mu_{(0)}, \lambda=\lambda_{(0)}}}_{<0} \geq -\mu_{(0)} \quad \forall \mu_{(0)} > 0 \quad (70)$$

$$\mu_{(1)} = \mu_{(0)} + \eta_0 \underbrace{\nabla_{\mu} \mathcal{F}|_{\mu=\mu_{(0)}, \lambda=\lambda_{(0)}}}_{>0} \leq -\mu_{(0)} \quad \forall \mu_{(0)} < 0 \quad (71)$$

For simplicity, to rule out the possibility of moving to $\mu_{(1)} = 0$ we further restrict the above conditions to prevent sign switching (this is sufficient but not necessary):

$$\mu_{(0)} + \eta_0 \underbrace{\nabla_{\mu} \mathcal{F}|_{\mu=\mu_{(0)}, \lambda=\lambda_{(0)}}}_{<0} > 0 \quad \forall \mu_{(0)} > 0 \quad (72)$$

$$\mu_{(0)} + \eta_0 \underbrace{\nabla_{\mu} \mathcal{F}|_{\mu=\mu_{(0)}, \lambda=\lambda_{(0)}}}_{>0} < 0 \quad \forall \mu_{(0)} < 0 \quad (73)$$

Re-arranging, we get:

$$\eta_0 < \frac{\mu_{(0)}}{-\nabla_{\mu} \mathcal{F}|_{\mu=\mu_{(0)}, \lambda=\lambda_{(0)}}} \quad (74)$$

$$= \frac{\mu_{(0)}}{\mu_{(0)}v(1 - \lambda_{(0)} + c\lambda_{(0)}) - \nabla_{\theta} MLL|_{\theta=\mu_{(0)}}} \quad (75)$$

$$= \frac{1}{v(1 - \lambda_{(0)} + c\lambda_{(0)}) - \frac{\nabla_{\theta} MLL}{\theta}|_{\theta=\mu_{(0)}}} \quad (76)$$

This clearly holds under condition 56. Thus we have so far demonstrated the following under the conditions of the proposition:

$$|\mu_{(1)}| = |\mu_{(0)} + \eta_0 \nabla_{\mu} \mathcal{F}|_{\mu=\mu_{(0)}, \lambda=\lambda_{(0)}}| < |\mu_{(0)}| \quad (77)$$

Now we show that if $|\mu_{(1)}| < |\mu_{(0)}|$, then we must have that $\lambda_{(1)} < \lambda_{(0)}$. This is trivially done using the CAVI update for λ :

$$\lambda^*(\mu) = \frac{1}{1 + c^{-\frac{1}{2}} e^{-\frac{1}{2}|\mu|^2 v(1-c)} \left(\frac{1-\pi_0}{\pi_0} \right)} \quad (78)$$

Therefore the gradient wrt. $|\mu|$ is:

$$\begin{aligned}\frac{d\lambda^*}{d|\mu|} &= \frac{|\mu|v(1-c)c^{-\frac{1}{2}}e^{-\frac{1}{2}|\mu|^2v(1-c)}\left(\frac{1-\pi_0}{\pi_0}\right)}{\left(1+c^{-\frac{1}{2}}e^{-\frac{1}{2}|\mu|^2v(1-c)}\left(\frac{1-\pi_0}{\pi_0}\right)\right)^2} \\ &= |\mu|v(1-c)\lambda^*(1-\lambda^*) \geq 0 \quad \forall \mu \neq 0, \pi_0 \in (0,1)\end{aligned}\tag{79}$$

This gradient is strictly positive when $|\mu| > 0$, $\lambda^* > 0$, $c > 0$. Thus we must have that $\lambda_{(t)} < \lambda_{(t-1)}$ if $|\mu_{(t)}| < |\mu_{(t-1)}| \quad \forall t \in \mathbb{Z}_+$.

Now since $\lambda_{(1)} < \lambda_{(0)}$, using the same steps as above we can similarly show under the conditions of the proposition that $|\mu_{(2)}| < |\mu_{(1)}|$ and $\lambda_{(2)} < \lambda_{(1)}$. Since the argument recurses for $t \in [T]$ iterations, for any $T \in \mathbb{Z}_+$, we have shown that under the conditions of Proposition 1, for some $\mu_{(0)}$ that induces $\lambda_{(0)} \leq \epsilon \in (0,1)$, we have:

$$|\mu_{(t)}| < |\mu_{(t-1)}| \dots < |\mu_0| \quad \forall t \in \mathbb{Z}_+ \tag{80}$$

$$\lambda_{(t)} < \lambda_{(t-1)} \dots < \lambda_{(0)} \quad \forall t \in \mathbb{Z}_+ \tag{81}$$

□

REMARK 2 Proposition 1 states that for a large enough spike precision v , small enough learning rate sequence $\{\eta_t\}_{t=0}^T$, and a small enough $|\mu_{(0)}|$ returned after the first approximate CAVI step for $q(\theta)$, we are guaranteed a sequence of monotonically decreasing a-CAVI updates $\{(|\mu_{(t)}|, \lambda_{(t)})\}_{t=0}^T$ for this restriction of the algorithm. This implies $\mu_{(t)}$ converges to a neighbourhood of zero in infinite computation time, and $\lambda_{(t)}$ converges to its minimum obtainable value given the optimal CAVI update in equation 34.

7.8.1 Implications for dropout pruning

The conditions in the proposition are strong but enable us to mathematically formalise the notion that if $\lambda_j \leq \epsilon$ for small enough $\epsilon \in (0,1)$ and large enough $v > 0$, then the KL regularisation effect can dominate the expected likelihood term $\langle \log p(\mathbf{y}|\theta) \rangle_{q_\psi(\theta)}$ during the remaining a-CAVI iterations, leading to $\mu_j \approx 0$ after many iterations. We observe this experimentally. This implies that performing dropout pruning on variables with $\lambda_j \leq \epsilon \in (0,1)$ may have negligible effect on the optimisation process and found local optimum, thus enabling us to enjoy its computational speed ups without notable performance loss.

Clearly the proposition is less likely to hold as n grows when using nearest neighbour minibatching, as the expected likelihood term contains a $\frac{n}{m}$ rescaling factor. In fact, this rescaling factor means that in the infinite sample limit the recovered parameters (μ, ϕ) under ZT posterior $q_\psi(\theta)$ should be no different than those recovered using the minibatch SGD procedure of Chen et al. (2020) i.e. the learned PIPs have no effect on $q_\psi(\theta)$.

In this case we motivate dropout pruning from the perspective of re-instating the link between $q(\gamma)$ and $q_\psi(\theta)$, as it essentially augments the evidence lower bound with an L0 regularisation penalty on μ_j with penalty scale $\lim_{\tau \rightarrow \infty} (\tau \delta_1(\lambda_j \leq \epsilon))$. Under dropout, small enough λ_j enforces $\mu_j = 0$ and only 'relevant' variables with $\lambda_j > \epsilon$ feature in LOO-LPD computation and predictions. This perspective is why we set the dropout pruning threshold to $\epsilon = 0.5$ (rather than a much smaller value). By doing so, we ensure that if the BMA procedure places all mass on a single model, the variables that influence predictions all have $\lambda_j \geq 0.5$. If we were to instead set $\epsilon \approx 0$ which increases the likelihood that Proposition 1 holds, then our BMA procedure can return model weights concentrated on a single model where we have $\lambda_j \approx 0 \quad \forall j \in [d]$.

8 Experimental and implementation details

Here we discuss in detail the experiments ran and settings used for all methods implemented. All results were run on a 2.70GHz Intel(R) Core(TM) i7-10850H CPU with 32MB RAM. All code for our SSVGP is written in Python and will be made publically available. Note that barring the toy example, when we refer to the SSVGP, we refer to using our Bayesian model averaging (BMA) procedure introduced in Section 4 of the main paper, where models are trained using a-CAVI Algorithm 1 with the zero-temperature posterior $q_\psi(\theta)$ and dropout

pruning procedure. The first toy example is used to demonstrate that our initial method (without BMA, zero-temperature and dropout) can perform well, but the adjustments are required for simultaneously reliable, fast and scalable performance.

8.1 Toy example

Here we consider the problem of identifying relevant variables in a high-dimensional synthetic dataset. We draw a univariate response from a sinusoidal function of 5 inputs corrupted with a small amount of noise:

$$y = f(\mathbf{x}) + \epsilon \quad (82)$$

$$f(\mathbf{x}) = \sum_{j=1}^5 \sin(a_j x_j) \quad (83)$$

$$\mathbf{x} \sim \mathcal{N}_d(0, I) \quad (84)$$

$$\epsilon \sim \mathcal{N}(0, \sigma^2) \quad (85)$$

We set $d = 100$ with $\{a_j\}_{j=1}^5$ grid spaced over $[0.5, 1]$ and draw datasets of size $n = 300$ using this generative process, controlling the noise variance to $\frac{1}{20}$ of the signal variance: $\sigma^2 = 0.05 \text{Var}[f(X)]$. Thus only 5/100 signals are relevant. Before running all methods we standardise $\mathcal{D} = (\mathbf{y}, X)$ to have mean zero and unit variance.

Our initial implementation of the SSVGP on this example uses a Mean-Field Gaussian approximation for inverse lengthscale posterior: $q_\psi(\boldsymbol{\theta}) = \mathcal{N}(\boldsymbol{\mu}, \text{Diag}(\sigma_1^2, \dots, \sigma_d^2))$ and fixed value of spike prior hyperparameter v . We train using $K = 5$ a-CAVI iterations with $T = 200$ gradient steps for the first a-CAVI iteration, and $T = 100$ steps thereafter. We use default ADAM smoothing parameters of $(\beta = 0.9, \beta_2 = 0.999)$ a learning rate of $\eta = 0.01$ and $S = 1$ Monte Carlo samples in reparameterisation gradient approximations. Prior hyperparameters are set as $(a, b, c, v) = (10^{-3}, 10^{-3}, 10^{-8}, 10^4)$ so that the spike precision $v = 10^4$ approximates a Dirac spike at zero, and the slab precision $cv = 10^{-4}$ approximates a uniform distribution. We initialise $\boldsymbol{\lambda} = \mathbf{1}$ (this is critical to avoid shrinking inverse lengthscales for relevant variables in the initialisation phase due to the regularisation of the KL term), and set $\boldsymbol{\xi} = \mathbf{1}$. We initialise inverse lengthscale posterior means to $\boldsymbol{\mu} = \mathbf{1} \times d^{-\frac{1}{2}}$ (this prevents numerical underflow in kernel evaluations in high-dimensional designs), and posterior variances to $\boldsymbol{\sigma} = 2 \times 10^{-3}$ and set $\boldsymbol{\phi} = \mathbf{1}$. We also add a jitter of 10^{-3} to the diagonals of K_{XX} .

The ML-II GP is implemented using the GPytorch (Gardner et al., 2018) library for 1000 iterations of ADAM with a learning rate of 0.1 and the same initialisation as our SSVGP for shared parameters. We use our own implementation of the Dirac spike and slab GP with paired mean field (PMF) approximation since there is no existing implementation in GP libraries (see Appendix 1 for mathematical model details). We run two versions with $S = 10$ and $S = 100$ Monte Carlo samples used respectively for score gradient estimation of $\nabla_{\boldsymbol{\lambda}} \mathcal{F}$. Since our implementation does not use control variates (Liu et al., 2019) or Rao-Blackwellisation (Salimans and Knowles, 2014) for variance reduction, we use the $S = 100$ sample version as an indication of obtainable performance using $S = 10$ samples were these techniques used, since Mohamed et al. (2020) find these can techniques can reduce variance by close to an order of magnitude in some experiments. We also optimise performance by a-priori fixing the prior inclusion probability to the true value ($\pi = 0.05$) and pre-tuning the slab precision $v_1 \in \{10^{-1}, 10^{-2}, 10^{-3}, 10^{-4}, 10^{-5}\}$. We train using the same number of total gradient iterations (500) and initialisation (for shared parameters) as the SSVGP except we initialise $\boldsymbol{\lambda} = 0.5$, which performed better than 1.

We subsequently re-implement the SSVGP (our final method) using the BMA procedure, zero-temperature posterior restriction and dropout pruning introduced in Section 4. We use 11 values of spike precision v grid-spaced over $\mathcal{V} = 10^4 \times 2^{\{-\log_2(1000), \log_2(1000)\}}$ such that $v \in [10, 10^7]$. We set the pruning threshold to $\epsilon = 0.5$ and use a slightly larger base learning rate of $\eta = 0.05$ (our default recommendation in small- n settings for our final method). We find this performs better in the absence of gradient variance due to the zero-temperature assumption. We use $m = \frac{n}{4}$ minibatching to further reduce runtime, and as we find this does not harm performance in our experiments. No nearest neighbour truncation of the LOO-LPD and predictive distribution is used.

We complete 10 trials of each method on synthetic dataset draws, reporting results in Tables 1 and 4 in the main text (we include test performance on $n_* = 100$ test points drawn from the same process). Figures 1 and 2 in the main text display average size ordered profiles for parameters that can be used to infer variable relevance for different methods (e.g. inverse lengthscales for the ML-II GP and PIPs for the SSVGP implementations). These profiles are constructed by size ordering the recovered parameters within each trial and then averaging the resulting profiles over the 10 trials. However we constrain the first 5 variables in the ordering (LHS of black

dashed line) to be selected from the 5 relevant variables. Thus, the 4th column in the variable ranking corresponds to the average value of the 4th largest parameter recovered amongst the relevant variables, and the 10th column corresponds to the average value of the 5th largest parameter recovered amongst the irrelevant variables.

These profiles enable us to clearly visualise the ability of our methods to better distinguish between irrelevant and relevant variables correctly vs. the ML-II GP. In particular, we see that the ML-II GP produces a smooth decline in the profile with no real discontinuity at the true inclusion/exclusion threshold, and fails to shrink the inverse lengthscales to arbitrarily small values (e.g. < 0.01) for the irrelevant dimensions (see Fig 1), making it very challenging to use thresholding reliably to do variable selection. By contrast, our SSVGP shows a huge discontinuity both in PIPs and (posterior mean) inverse lengthscales at the true inclusion cut-off (see Fig. 2), and also learns to include all relevant variables with PIP ≈ 1 and include all irrelevant variables with PIP $\ll 0.5$.

8.1.1 Analysis of posterior point of intersection (PPI)

In Section 4 we demonstrated the sensitivity of the a-CAVI algorithm recovered PIPs to the value of spike and slab hyperparameter v . We also argued that the root of the problem is that the posterior point of intersection (PPI) is generally much more insensitive to $q(\pi)$ (which adapts the PPI during a-CAVI iterations) than to v . Recall that the PPI is the value of the transformed expected sufficient statistic of the inverse lengthscale $\hat{\theta} = \langle \theta^2 \rangle_{q_{\psi_j}(\theta)}$ that induces an even probability of inclusion for variable j in the CAVI update for $q(\gamma_j)$:

$$\hat{\theta} = \sqrt{\frac{\log\left(\frac{1}{c}\right) + 2\langle \log\left(\frac{1-\pi}{\pi}\right) \rangle_{q(\pi)}}{v(1-c)}} \quad (86)$$

To demonstrate the relative sensitivity to $q(\pi)$ and v , below in Figure 7 we display how the PPI varies with π_0 and v (under the restriction that $q(\pi) = \delta_{\pi_0}(\pi)$ for simplicity). As we can see, unless π_0 is extremely small or large, the PPI varies minimally over π_0 but varies substantially with v (the PPI is $\mathcal{O}(v^{-\frac{1}{2}})$). Thus v can entirely determine the sparsity of the learned PIPs λ .

The other issue is that the range of PPI values that give good variable selection accuracy may vary based on the function properties, and so it is not the case that a single value of v will perform well across all designs. For example, a function that varies much more slowly may require a lower PPI to prevent false exclusions of small but relevant inverse lengthscales.

To demonstrate this, we display on Figure 8 below the PIP profiles recovered on the 10 trials of the toy example using our SSVGP with a Mean-Field Gaussian posterior, for two fixed values of v (10^4 and 10^5), as well as for our final method (SSVGP+BMA with zero-temperature and dropout pruning). We also display on Fig. 9 an equivalent set of profiles recovered on a modified version of the generative process where now 25/100 variables are relevant $\{a_j\}_{j=1}^{25}$ are grid spaced over $[0.05, 0.1]$. Whilst $v = 10^4$ performs well on the original design, but poorly on the second design, the opposite holds for $v = 10^5$. However the BMA procedure is able to effectively adapt the PPI so that the PIPs more accurately reflect each generative design.

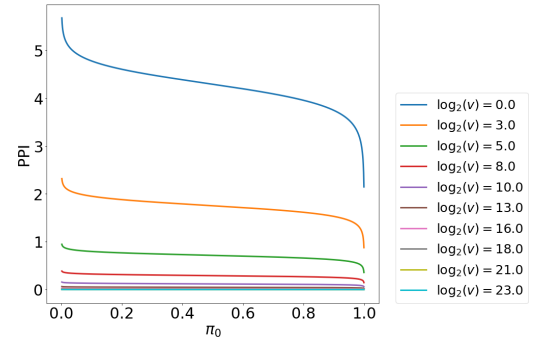


Figure 7: Posterior point of intersection (PPI) over 10 values of v grid spaced over $10^{\{0, \dots, 7\}}$ and 1000 values of π_0 grid spaced over $[0.001, 0.999]$.

8.2 Experiment 1

We next test our SSVGP on 50 trials of the additive function used in Savitsky et al’s (2011) main high-dimensional experiment. They use this experiment to test their MCMC algorithm for the spike and slab GP. Since spike and slab priors with a Dirac spike and MCMC for posterior inference is considered a gold-standard in Bayesian variable selection (Narisetty and He, 2014), if our SSVGP can perform similarly well to their algorithm, we can be confident that our method can compete with best practice (but in a tiny fraction of the runtime). They were only able to complete a single trial of their method as they required 800,000 MCMC iterations to ensure sufficient mixing of the chain (first 400,000 discarded as burn-in). We note that they do not produce the runtime

of their trial, but they do produce a runtime of 10224s when running the same algorithm for 500,000 iterations on an identically sized dataset ($n = 100, d = 1000$). Thus, we conclude with confidence that their runtime for the main high-dimensional experiment is likely to be $> 10000s$.

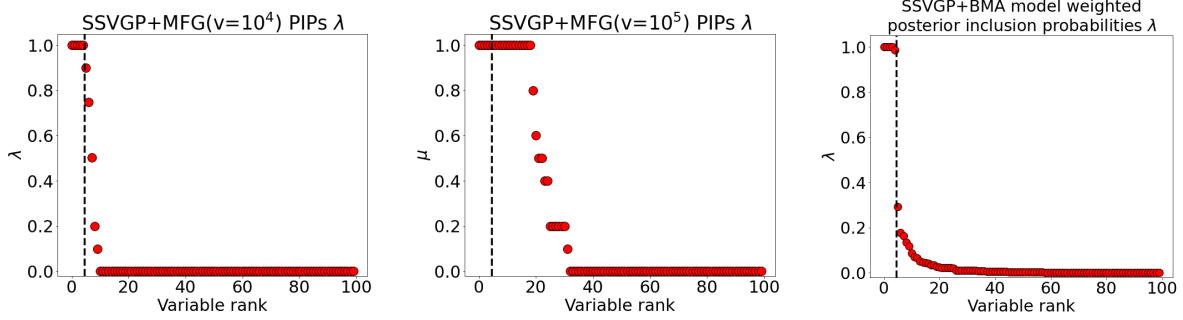


Figure 8: Toy example size ordered PIP profiles (averaged over 10 trials) using the original design (5 relevant variables) for SSVGP with (LHS) Mean-Field Gaussian and fixed $v = 10^4$, (Center) Mean-Field Gaussian and fixed $v = 10^5$, (RHS) BMA with zero-temperature posterior (our final method). Profiles are constructed by size ordering the PIPs per trial with $q = 5$ relevant variables constrained to take the first q places in the ordering (LHS of black dashed line), and averaging the resulting profiles over the trials. $v = 10^4$ performs much better than $v = 10^5$, but doing BMA over 11 values of v grid spaced over $10^4 \times 2^{\{-\log_2(1000), \log_2(1000)\}}$ performs best.

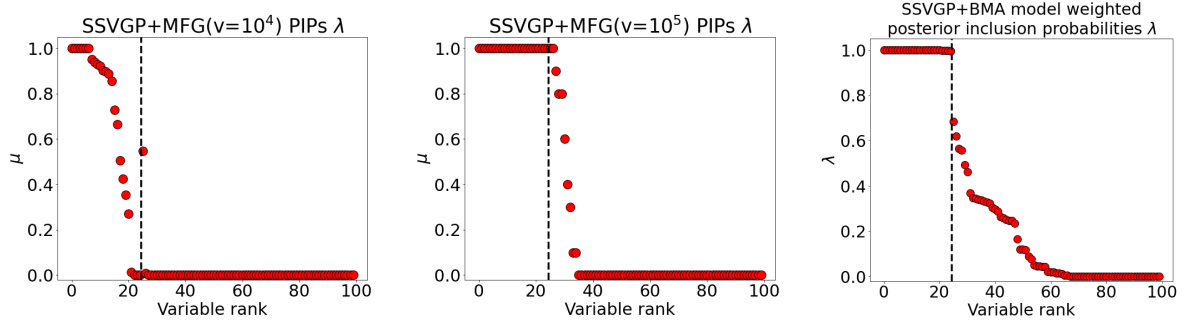


Figure 9: Toy example average size ordered PIP profile using the modified design (25 relevant variables) for SSVGP with (LHS) Mean-Field Gaussian and fixed $v = 10^4$, (Center) Mean-Field Gaussian and fixed $v = 10^5$, (RHS) BMA with zero-temperature posterior. By comparison with Fig. 8, $v = 10^5$ performs better than $v = 10^4$. However BMA performs best again, demonstrating its ability to effectively adapt to the generative process.

The experiment draws $n = 100$ training samples and $n_* = 20$ test samples from the following generative process:

$$y = x_1 + x_2 + x_3 + x_4 + \sin(3x_5) + \sin(5x_6) + \epsilon \quad (87)$$

$$\epsilon \sim \mathcal{N}(0, 0.05^2) \quad (88)$$

$$\mathbf{x} \sim \mathcal{U}[0, 1]^{1000} \quad (89)$$

Thus, 6/1000 input variables are relevant. We implement our SSVGP (from now on with BMA, zero-temperature and pruning) and the ML-II GP using exactly the same implementation settings as in the toy example. We use three minibatch sizes of $m \in \{\frac{n}{4}, \frac{n}{2}, n\}$ to test how this affects performance. We also implement the following models with embedded variable selection: (LASSO (Tibshirani, 1996), MCP (Zhang, 2010), GAM with group LASSO penalty (Huang et al., 2009) and GAM with group spike and slab LASSO (SS LASSO) penalty (Bai et al., 2020). The LASSO and MCP were implemented using the R `ncvreg` package (Breheny and Breheny, 2021), the GAM LASSO and GAM spike and slab LASSO (SS) were implemented using the R package `sparseGAM` (Bai, 2021). In all cases default cross-validation procedures were used except for the GAM SS LASSO where

3 fold CV was used to keep runtimes manageable. All code was ran using the `rpy2` library in Python. We standardise inputs to have zero mean and unit variance following Savitsky et al. (2011).

Fig. 3 in the main text presents mean-squared error (MSE) and runtime performance percentiles for 50 trials of the experiment. We measure variable selection accuracy using the Matthews Correlation Coefficient (MCC $\in [-1, 1]$) - a best practice measure of imbalanced classification accuracy (Chicco and Jurman, 2020). We select using a PIP threshold of $\bar{\lambda} = 0.5$ with the SSVGP. For the ML-II GP we report MCC performance using the *best* performing threshold from $0.1^{0.5, 1, 1.5, 2}$, as indicative 'best-case' performance achievable with inverse lengthscale thresholding. All other methods automatically do binary variable selection. We report performance percentiles instead of mean and standard deviation as we found the distribution to be heavily skewed by a few outlier trials with poor performance. Detailed performance for different percentiles is contained in Table 6 below. For transparency, we additionally display the mean and standard deviation performance below in Table 8, but note the large standard deviations reflecting the outliers. We normalise the mean-squared error by the variance of the response as in Savitsky et al (2011).

	25 th percentile			50 th percentile			75 th percentile		
	MSE	MCC	Runtime	MSE	MCC	Runtime	MSE	MCC	Runtime
SSVGP(m=n)	0.0046	1	19.6	0.0082	1	19.9	0.0133	0.93	20.5
SSVGP(m=n/2)	0.0043	1	10.4	0.0068	1	10.6	0.0111	1	11.1
SSVGP(m=n/4)	0.005	1	7.9	0.0086	1	8.2	0.0125	1	8.7
ML-II GP	0.0843	0.82	3.8	0.1321	0.77	3.9	0.1817	0.72	4
GAM SS LASSO	0.2749	1	386.7	0.3563	0.93	390.1	0.4831	0.82	393.6
GAM LASSO	0.0725	0.53	3.8	0.1373	0.43	3.9	0.1849	0.4	4.1
LASSO	0.3777	0.44	0.3	0.4796	0.35	0.3	0.6254	0.3	0.3
MCP	0.2731	0.64	0.3	0.3755	0.54	0.3	0.4815	0.49	0.4

Table 6: Experiment 1 performance percentiles for implemented models. Bold indicates best performing method per column. Note that the percentiles are reported such that the 75th percentile performance is worse than the 25th percentile performance, regardless of the metric. All SSVGP implementations outperformed the comparator set in variable selection and predictive accuracy for all percentiles reported.

	MSE	MCC	Runtime (s)
Savitsky et al (2011) MCMC spike and slab GP (single trial)	0.0067	1	>10000

Table 7: Single trial performance of Savitsky et al’s (2011) single trial of their MCMC spike and slab GP on the high-dimensional experiment. MSE is mean squared error and MCC is Matthews Correlation Coefficient. Note that they do not report a runtime for this specific trial, where they ran for 800,000 MCMC iterations. However they do report a runtime of 10224s on an identically sized experiment where they used 500,000 iterations. Thus we conclude with confidence that the runtime must have exceeded 10000s.

	MSE	MCC	Runtime
SSVGP($m=n$)	0.0616 ± 0.1267	0.85 ± 0.25	20.3 ± 1.2
SSVGP($m=n/2$)	0.0187 ± 0.0422	0.94 ± 0.16	11.0 ± 0.9
SSVGP($m=n/4$)	0.0258 ± 0.0543	0.93 ± 0.17	8.4 ± 0.6
ML-II GP	0.143 ± 0.0933	0.79 ± 0.13	3.9 ± 0.2
GAM SS	0.4174 ± 0.2154	0.87 ± 0.14	389.9 ± 4.8
GAM LASSO	0.164 ± 0.138	0.47 ± 0.1	4.0 ± 0.2
LASSO	0.5065 ± 0.1548	0.37 ± 0.1	0.3 ± 0.0
MCP	0.4103 ± 0.1885	0.58 ± 0.11	0.3 ± 0.0

Table 8: Experiment 1 mean \pm standard deviation performance for implemented models. MSE is mean squared error and MCC is Matthews Correlation Coefficient. Bold indicates best performing method per column. All SSVGP implementations outperformed the comparator set on average variable selection and predictive accuracy, with the exception that the GAM spike and slab lasso of [Bai et al. \(2020\)](#) marginally outperformed the SSVGP with $m = n$ on average with respect to variable selection accuracy (MCC). However this is mostly due to several outlier trials with poor performance for the SSVGP($m=n$), which skews the average MSE and MCC.

8.3 Experiment 2

Here we test the scalability and predictive accuracy of our SSVGP in a large-scale sparse input prediction challenge. The aim of this experiment is to demonstrate that regardless of whether variable selection is a central task, our method can substantially improve on the predictive performance of benchmark scalable GP approximations by taking advantage of input relevance sparsity when available. In this experiment we draw a univariate response from the following interactive function of two inputs:

$$y(\mathbf{x}) = f(\mathbf{x}) + \epsilon \quad (90)$$

$$f(\mathbf{x}) = \tan(x_1) + \tan(x_2) + \sin(2\pi x_1) + \sin(2\pi x_2) + \cos(4\pi^2 x_1 x_2) + \tan(x_1 x_2) \quad (91)$$

$$\epsilon \sim \mathcal{N}(0, \sigma^2) \quad (92)$$

$$(x_1, x_2) \sim \mathcal{U}[0, 1]^2 \quad (93)$$

We then augment the dataset with $d - 2$ noise dimensions \mathbf{z} , where $\text{corr}(x_i, z_j) = \text{corr}(z_j, z_k) = 0.5 \quad \forall i \in [2], \quad \forall j, k \in [d - 2]$. To generate this correlation structure we pass \mathbf{x} through an inverse standard Gaussian CDF, draw $\mathbf{z}|\mathbf{x}$ using standard Gaussian conditioning formulae, and then pass \mathbf{x}, \mathbf{z} back through a standard Gaussian CDF. We fix $nd = 10^8$ and consider two variations in dimensions: (1) an ultra-high dimensional design ($n = 10^4, d = 10^4$) and (2) a one million training point design ($n = 10^6, d = 10^2$). For testing we draw an equivalent dataset of size $n_* = 10^4$ using the same generative process, but now with x_1, x_2 as grid spaced over $[0, 1]$. This enables a 2d prediction surface to be produced as a function of the two generating inputs and thus facilitates clear visual comparisons in results.

We implement the SSVGP using the same implementation settings as previously but use a smaller base learning rate of $\eta = 0.01$. We use the smaller learning rate in large- n designs when using minibatch sizes such that $m \ll n$, as we find this leads to more stable learning due to the high degree of gradient variance. The specific minibatch sizes we choose are $m \in \{64, 128, 256\}$. We constrain the nearest neighbours in the minibatch to be chosen from a random subset of $\min(n, 10^4)$ datapoints to limit the per-iteration nearest neighbour search cost. We nearest neighbour truncate the LOO-LPD using $\tilde{m} = 64$ neighbours, and the predictive distribution using $m_* = 256$ neighbours. We find $\tilde{m} \leq 64$ is required for competitive runtimes when $n = 10^6$ and $m_* \geq 256$ is required for (near) optimal predictive performance vs. using $m = n$. We consider $\tilde{m} = 64$ and $m_* = 256$ as default recommendations for our method. We use KD-trees ([Bentley, 1975](#)) whenever the active input dimensionality is $d < 100$, else we use Ball trees ([Omohundro, 1989](#)).

Since the experiment is focussed on predictive accuracy, we also do the following to speed up computation time: (i) We select the best model rather than averaging as this means only one set of GP predictive moments are computed, and (ii) We compress the model set such that if any M models select the same variables, we keep only the model $i \in [M]$ with the best LOO-LPD on a random subset of $n = 1000$ training points. This leads to substantial time savings when $n = 10^6$, since as $n \rightarrow \infty$ LOO-LPD dominates computation time due to its superlinear complexity. These are default recommendations when predictive accuracy is the main concern.

The two competitors we use are the sparse Gaussian process (SGP) of Titsias (2009), and the stochastic variational Gaussian process (SVGP) of Hensman et al. (2013), which are popular benchmarks in the scalable GP literature. We follow the implementations in Wang et al. (2019); Chen et al. (2020) (512/1024 inducing points, 100 iterations/epochs and an ADAM learning rate of 0.1/0.01 for the SGP/SVGP respectively). However we deviate from this in the following cases : (1) In the ultra-high-dimensional design we train for 200 iterations/epochs as performance was extremely uncompetitive after 100 iterations/epochs. (2) In the one-million training point design we use 25 epochs for the SVGP as we found this did not change predictive accuracy noticeably but enabled 4 \times savings in runtime (runtimes were not competitive for the SVGP when $n = 10^6$ using 100 epochs otherwise). We also use natural gradients for the SVGP following the GPytorch documentation recommendations. We use the same initialisation as our SSVGP for shared parameters, and standardise inputs and the response as previously.

Mean and standard deviation performance results from 3 trials of each design are in Fig. 5 in the main text. We also display in Fig. 4 of the main text the average prediction surfaces as a function of the two generating inputs for each method, against the true (noiseless) latent test surface \mathbf{f}_* . Full results tables and a breakdown of the runtime source for our SSVGP are below in Tables 9-10. Our SSVGPs all performed best on average and kept competitive runtimes in both designs (faster than both comparators when $n = 10^6$ and faster than the SVGP when $n = 10^4$). We note the relatively faster runtimes achieved by our method in the $n = 10^6$ case do not reflect better complexity with respect to n , but rather that more models in the BMA ensemble selected the same variables and thus the collapsed the model set was smaller for LOO-LPD computation.

In the ultra-high-dimensional design ($n = d = 10^4$), runtime is dominated by a-CAVI training time, and the larger minibatch size therefore substantially increases total time. However in the one-million training point design ($n = 10^6, d = 10^2$), the runtime is dominated by LOO-LPD computation due to its superlinear complexity. In this case, we actually find $m = 256$ runs fastest on average, as it tended to prune (select) fewer variables per BMA ensemble member (recall LOO-LPD compute time is linear in the number of non-pruned variables p_k per model \mathcal{M}_k in the BMA ensemble).

	$(n = 10^4, d = 10^4)$		$(n = 10^6, d = 10^2)$	
	MSE	Runtime (mins)	MSE	Runtime (mins)
SGP(512)	0.682 ± 0.015	$\mathbf{14.1} \pm 0.3$	0.263 ± 0.002	288.7 ± 17.2
SVGP(1024)	0.644 ± 0.005	154.8 ± 3.3	0.256 ± 0.002	365.6 ± 14.9
SSVGP(m=256)	0.26 ± 0.002	42.6 ± 5.9	0.251 ± 0.002	227.3 ± 23.2
SSVGP(m=128)	0.261 ± 0.003	24.3 ± 4.3	0.251 ± 0.002	236.6 ± 15.6
SSVGP(m=64)	0.262 ± 0.004	17.9 ± 2.9	0.251 ± 0.002	245.8 ± 17.0

Table 9: Experiment 2 mean \pm standard deviation results (MSE = mean squared error) from 3 trials on the two dataset sizes tested. Bold indicates the best performing method.

	$(n = 10^4, d = 10^4)$			$(n = 10^6, d = 10^2)$		
	Train	LOO-LPD	Test	Train	LOO-LPD	Test
SSVGP(m=256)	35.4 ± 2.4	6.9 ± 3.5	0.2 ± 0.0	11.9 ± 0.2	215.0 ± 23.2	0.4 ± 0.0
SSVGP(m=128)	17.3 ± 0.7	6.7 ± 3.6	0.2 ± 0.0	12.3 ± 0.2	223.9 ± 15.4	0.3 ± 0.0
SSVGP(m=64)	12.9 ± 0.7	4.8 ± 2.3	0.2 ± 0.0	12.1 ± 0.3	233.3 ± 16.7	0.3 ± 0.0

Table 10: Experiment 2 mean \pm standard deviation runtime (minutes) breakdown into training time (a-CAVI), LOO-LPD computation, and test time from 3 trials on the two dataset sizes tested.

8.4 Real datasets from UCI repository

We now test on two benchmark real datasets from the UCI repository with high-dimensional inputs ($d \gg 100$): CTSLICE ($n=53500, d=380$) and UJINDOORLOC ($n=21048, d=520$). As variable selection accuracy cannot be verified here we focus again on the predictive accuracy and runtime of our method. We implement the SSVGP against the SGP and SVGP using exactly the implementation settings as in Experiment 2 but train the SGP and SVGP using the default 100 iterations/epochs and set the SSVGP’s training minibatch to $m = 256$ (the best performing in Experiment 2). We run these methods on 10 trials of random splits into training and test sets, with 4/5 used for training. As previously we standardise the data to have mean zero and unit variance. We also

pass \mathbf{y} through a Box-cox transformation due to the heavy skew in the distributions, to maximise consistency with the Gaussian modelling assumptions. Fig. 6 in the main text contains the mean and standard deviation of MSE and runtimes obtained, and we display results tables below in 11. We also highlight in Fig. 10 below the ‘sparsity’ of the learned solutions by our SSVGP by comparison to the SGP/SVGP by comparing the recovered inverse lengthscales (post. mean used for SSVGP).

	CTSLICE (n=53500,d=385)			UJINDOORLOC (n=21048,d=520)		
	MSE	Runtime	Variables used	MSE	Runtime	Variables used
SSVGP(m=256)	0.003 \pm 0.001	34 \pm 2	142 \pm 25	0.027 \pm 0.003	18 \pm 0	170 \pm 32
SGP(512)	0.006 \pm 0.000	3 \pm 0	385	0.038 \pm 0.003	1 \pm 0	520
SVGP(1024)	0.005 \pm 0.000	60 \pm 1	385	0.035 \pm 0.003	25 \pm 0	520

Table 11: Real dataset results for our for our SSVGP with $m = 256$ minibatching, against SGP (Titsias, 2009) and SVGP (Hensman et al., 2013) on the real datasets. ‘Variables used’ is measured by the number of dimensions $j = (1....J)$ which affect predictions when $x_{*(j)}$ varies. Bold indicates the best performing method per column.

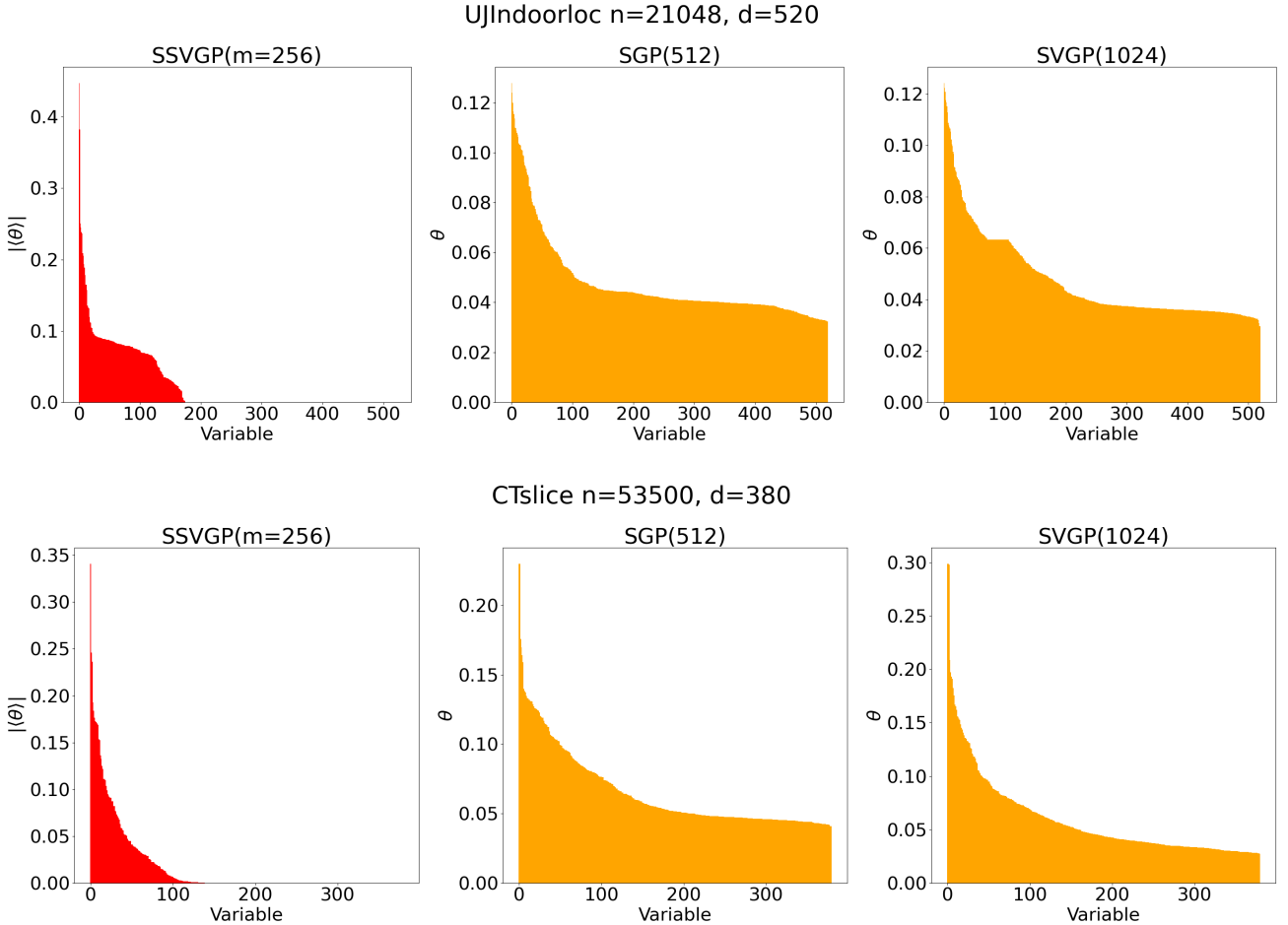


Figure 10: Size ordered inverse lengthscale profiles for our SSVGP with $m = 256$ minibatching (posterior mean of $q_\psi(\boldsymbol{\theta})$ used), against sparse GP (Titsias, 2009) and stochastic variational GP (Hensman et al., 2013) on the real datasets. Since our SSVGP is parameterised such that $\boldsymbol{\theta} \in \mathbb{R}^d$, we plot $|\langle \boldsymbol{\theta} \rangle_{q_\psi(\boldsymbol{\theta})}|$. The median trial is used to construct the profiles, meaning that the k^{th} column value is the median value of the k^{th} largest inverse lengthscale recovered. We use the median to indicate how the profile looks for a ‘typical’ trial, as the average is skewed by two trials with a larger number of selections. Our SSVGP learns an L0-sparse subset of inverse lengthscales through the BMA weighting over different models with varying aggressiveness in dropout pruning, but predicts with significantly more accuracy on average (see Table 11).